Ph. D. DISSERTATION

ANALYSIS ON OPERATIONAL STABILITY FOR STABLE QUANTUM DOT LIGHT-EMITTING DIODES

양자점 발광 다이오드 구동 안정성 연구

BY

SEUNGHYUN RHEE

FEBRUARY 2020

DEPARTMENT OF
ELECTRICAL AND COMPUTUER ENGINEERING
COLLEGE OF ENGINEERING
SEOUL NATIONAL UNIVERSITY

ANALYSIS ON OPERATIONAL STABILITY FOR STABLE QUANTUM DOT LIGHT-EMITTING DIODES

양자점 발광 다이오드 구동 안정성 연구

지도교수 곽 정 훈

이 논문을 공학박사 학위논문으로 제출함

2020 년 2 월

서울대학교 대학원

전기정보 공학부

이 승 현

이승현의 공학박사 학위논문을 인준함

2020 년 2 월

위 원 장 : 홍 용 택 (인)
부위원장 : 곽 정 훈 (인)
위 원 : 이 재 상 (인)
위 원 : 배 완 기 (인)
위 원 : 노 정 균 (인)

Abstract

ANALYSIS ON OPERATIONAL STABILITY FOR STABLE QUANTUM DOT LIGHT-EMITTING DIODES

SEUNGHYUN RHEE
DEPARTMENT OF ELECTRICAL AND COMPUTER ENGINEERING
COLLEGE OF ENGINEERING
SEOUL NATIONAL UNIVERSITY

Colloidal quantum dot light-emitting diodes (QLEDs) are p-i-n junction diodes exhibiting excellence in color gamut, brightness and flexible form factors, promising their use in next-generation displays. Within the last few decades, QLEDs have demonstrated great progress in efficiency and brightness that are comparable to the performance of commercialized organic light-emitting diodes (OLEDs) are reported.

To enhance performance of QLEDs, lots of attempts have been made on QD and QLED, such as modifying core/shell composition and structure, surface ligand modification, and optimization QLEDs device architectures. Through these methods,

tremendous improvement in terms of photoluminescence quantum yields (PL QY) of QDs and external quantum efficiency (EQE) of QLEDs have been accomplished. However the origin of key factors that reduces operational stability of QLEDs is still miles behind. There have been studies related to enhancement of QLEDs lifetime by insertion of blocking layer to prevent acidity of hole transport layer (HTL) or improving electron-hole balance by modifying device structure, but the mechanism of optical and electrical deterioration of the devices is still insufficient.

For the practical use of QLED, it is prerequisite to identify the relation between device operation conditions (Applied current density, voltage, and charge balance factors) and QLED lifetime. However lifetime analysis of the QLEDs, which have different structures (QDs or charge transport layer), leads unreliable comparison results due to the different operating conditions.

In this study, we improved QLEDs lifetime and performance with enhanced hole transport property by insertion of thin fullerene (C_{60}) as hole injection interlayer between CBP (HTL) and MoO_x layer (HIL, Hole injection layer). Insertion of buffer layer which has deep highest occupied molecular orbital (HOMO) level such as C_{60} can eliminate pinning effect between CBP and MoO_x layer. This eventually increase hole transport property in QLEDs and enhance balance of electron and hole transport rate to QD emissive layer. To clarify the relation between operational condition and lifetime of QLED, we quantitatively conduct the comparison between electrical properties of QLEDs and photophysical properties of the QD emissive layer within the devices under various operation condition. As these analytic researches are taken in the QLEDs which have nearly identical structure, the result shows intuitive understanding on the effect of operational condition in QLEDs.

As a result, the QLEDs with C_{60} interlayer showed 10% reduced initial rapid luminance drop compared to non-C_{60} interlayer QLEDs which leads to 5 times

increase in operational lifetime at 1000 nit. (75% lifetime (LT_{75}) ~ 5.6 hours @ 1000 cd/m^2 for non-C_{60} interlayer QLEDs and (LT_{75}) ~ 36.5 hours @ 1000 cd/m^2 for C_{60} interlayer QLEDs).

Comprehensive study across spectroscopic analysis on the QD emissive layer and optoelectronic characterization on working devices under all-else-being-equal operation conditions enable us to understand the key factors that are responsible for the device degradation. The device efficiency drop at Stage I is attributed solely to the charge injection imbalance into QDs. The device efficiency loss at Stage II is also attributed mainly to the charge injection imbalance, and further exacerbated by the increase in the operation voltage.

These results shows the impact of charge injection balance on the device performance, and suggest that the equalized charge injection will enable complete eradication of device degradation factors and promise prolonged operation lifetime of QLEDs.

I believe that engineering at the interface between QDs and HTL will certainly enable the complete charge injection balance and a long-lived QLED.

Keywords: Quantum Dot Based Light-Emitting Diodes, Operational Stability, Charge Injection Balance, Hole Injection Barrier, Fullerene.

Student Number: 2014-21662

Contents

List of Figures

List of Tables

Chapter 1

Introduction

1.1 Colloidal Quantum Dot Light-Emitting Diodes

Colloidal quantum dot (QD) based light-emitting diodes (QD-LEDs) are p-i-n junction diodes, in which electrically pumped charged carriers recombine within QDs to generate photons [1-9]. By exploiting advantageous features, quantum dot have applied to widespread fields such as displays [10, 11], lighting [12], lasing [13-16], solar cells [17, 18], bio-imaging [19], and sensor applications. Especially, QD-LEDs exhibit excellence in color gamut and brightness, and light-weight and flexible form factors, promising their use in next-generation displays and lightings [20]. After the first demonstration by V.L Colin and Louis Brus [3, 10], QD-LEDs have evolved to equip with high efficiency and brightness [1, 9, 13, 16], and recently QD-LEDs with near unity efficiency [21, 22] and high brightness [23] that are comparable to the performance of commercialized liquid crystal display (LCD) and organic light-emitting diodes (OLEDs).

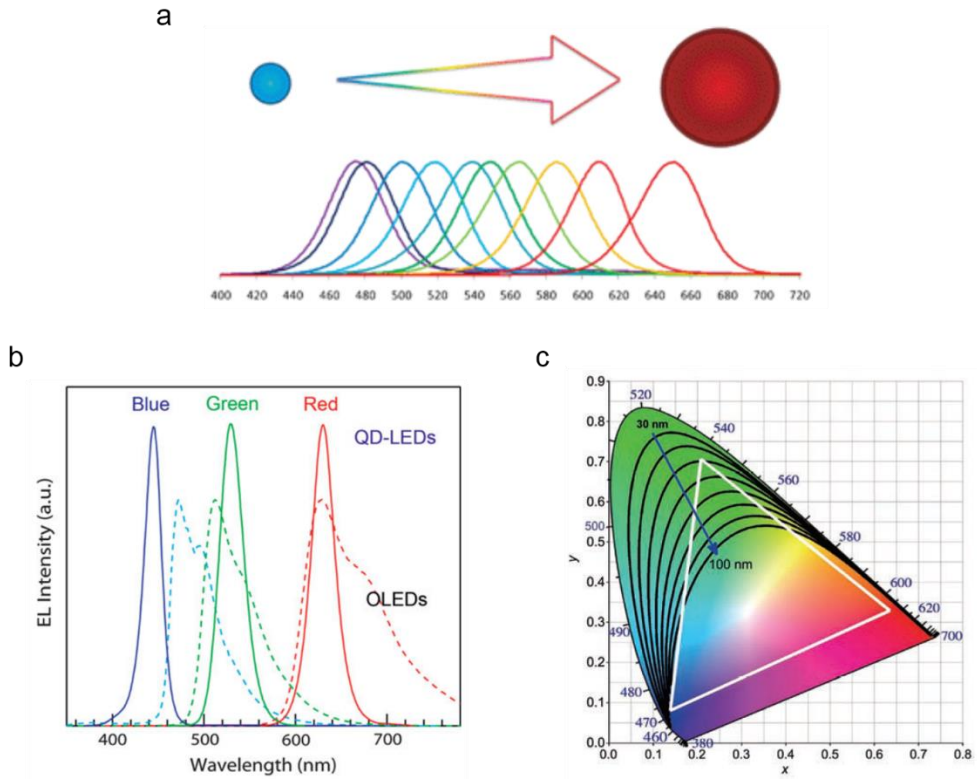

Figure 1.1 (a) Wavelength-tunable characteristics of QDs. By varying the chemical composition and nanoparticle size, quantum dots can illuminate all visible wavelength region [24]. (b) Comparison of red, green and blue EL spectra with (dashed lines) OLEDs and (solid lines) QD-LEDs [25]. (c) The CIE (Commission Internationale de l'Eclairage) 1931 chromaticity diagram. As full-width-half-maximum of the quantum dot narrows from 60 to 25 nm, the simulated spectral locus grows close to the edge of the CIE diagram. Simulations assume a Gaussian QD emission profile. [26].

Compared to the OLEDs, which has similar device structure and already commercialized, QD-LEDs has its own superior features. First, QDs can make all

visible region wavelength emission by modifying the chemical composition of core/shell structure and controlling the size of nanoparticles (Figure 1.1a). Second, although OLEDs show numerous progress, the broad width of the electroluminescence (EL) emission band is a drawback of the OLED technology. Full-width at half-maximum (FWHM) of OLEDs is greater than 40 nm due to the vibronic states of organics dyes. On the other hand, QDs exhibit narrow (less than 30 nm) emission spectra of FWHM due to its quantum mechanical features. Figure 1.1b shows the narrow EL spectra of QD-LEDs compared to that of typical OLEDs. Last, the narrow bandwidth feature of QD emitter leads to widening of the color reproducible range in the color gamut. (Figure 1.1c). These virtues in QDs make QD-LEDs as high color purity and excellence in color gamut, which is better than most of commercialized displays, and as convincing candidate for next-generation display and light source.

The progress of QD-LED performance is presented in Figure 1.2. Starting with simple device structure of indium tin oxide (ITO)/poly(p-paraphenylene vinylene) (PPV)/CdSe QDs/Mg by V.L Colin *et al.* [3], the EQE of QLEDs is now reached over 30 %, which is satisfied the requirements for displays. Numerous efforts have been made to enhance device performance. S. Coe *et al.* applied tris-(8-hydroxyquinoline) aluminium (Alq3) as ETL and N,N'-diphenyl-N,N'-bis(3-methylphenyl)-1,1'-biphenyl)-4,4' -diamine (TPD) as HTL for efficiency electron and hole injection into the QD emissive layer. This first demonstrated ETL/QD emissive layer/HTL structure, which is now formal matrix of QD-LED structure, improved 25-fold of luminescence efficiency (1.6 cd/A at 2,000 cd/m^2) compared to the previous QD-LED results [2]. Although they introduced 3-(4-biphenylyl)-4-phenyl-5-*t*-butylphenyl-1,2,4-triazole (TAZ) hole blocking layer (HBL) to reduce an adjacent layer peak from Alq3, the result still showed small parasitic peak from ETL and HTL due to incomplete exciton

energy transfer from the TPD HTL to the QD emissive layer. To isolated QD luminescence process and charge transport, the research on the modification of HTL, ETL, and QDs has been reported substantially. Changing the size of QD or ligand improved charge injection property and packing density of QDs [27] and various doping or bilayer structure of CTL controlled electron and hole injection into QDs emissive layer [28, 29]. J. Kwak *et al.* reported a new device architecture, i.e., an inverted structures which introduce ZnO nanoparticles as bottom ETL and thermally evaporated small molecules as HTL [5]. This inverted structure has broadened the number of hole transport material, introducing a new types of solution to resolve to hole injection difficulty in QD-LEDs. Since then, both conventional structure and inverted structure have been made great progress in efficiency and lifetime. Based on this progress, cd-based green and blue QD-LEDs reached near theoretical limit value (20 %) and cd-based red QD-LEDs reached even high value, 30 % [9, 30, 31]. J. Song *at el.* and H. Shen *at el.* high efficient red and green QD-LEDs by modification of QDs chemical architecture. J. Song *at el.* inserted intermediate ZnSe layer with an ultrathin ZnS outer layer as the shell materials and introduced 2-ethylhexane-1-thiol as ligand, resulting dramatic improvement of hole injection efficiency and thus lead to high balanced charge injection. By placing the emission zone at a quarter wavelength away from the reflector, which maximize the light interference enhancement in light extraction, they exceeded the ever reported theoretical efficiency limit (20 %) and achieved above 30 % EQE of red QD-LEDs. Similarly, H. Shen *at el.* accomplished high efficiency of green QD-LEDs by using ZnSe as the shell material and the presenting of Se throughout the CdSe/ZnSe core/shell regions. This method results high-quality interfaces, balanced charge injection and high current density at low voltage due to the easy accessing of hole injection in the devices. As

such, the drastic improvement of device efficiency, which is fully qualified for commercialize criteria, indicates QD-LEDs as future display applications.

Besides, non Cd-based QD-LEDs also showed great progress within few years. Recently, C. Ippen *at el.*, the members of Nanosys and LG Display reported high efficiency non Cd-based QD-LEDs with EQE = 16.9 %, 13 %, 9 % for red, green, and blue, respectively [32]. By optimizing the efficient InP-based QDs shell thickness, the device EQE initially improves because of the better charge confinement and reduced energy transfer among the QDs. The non Cd-based QD-LEDs is essential for a viable long-term solution for next generation displays and its device performance for commercialization nearly achieved.

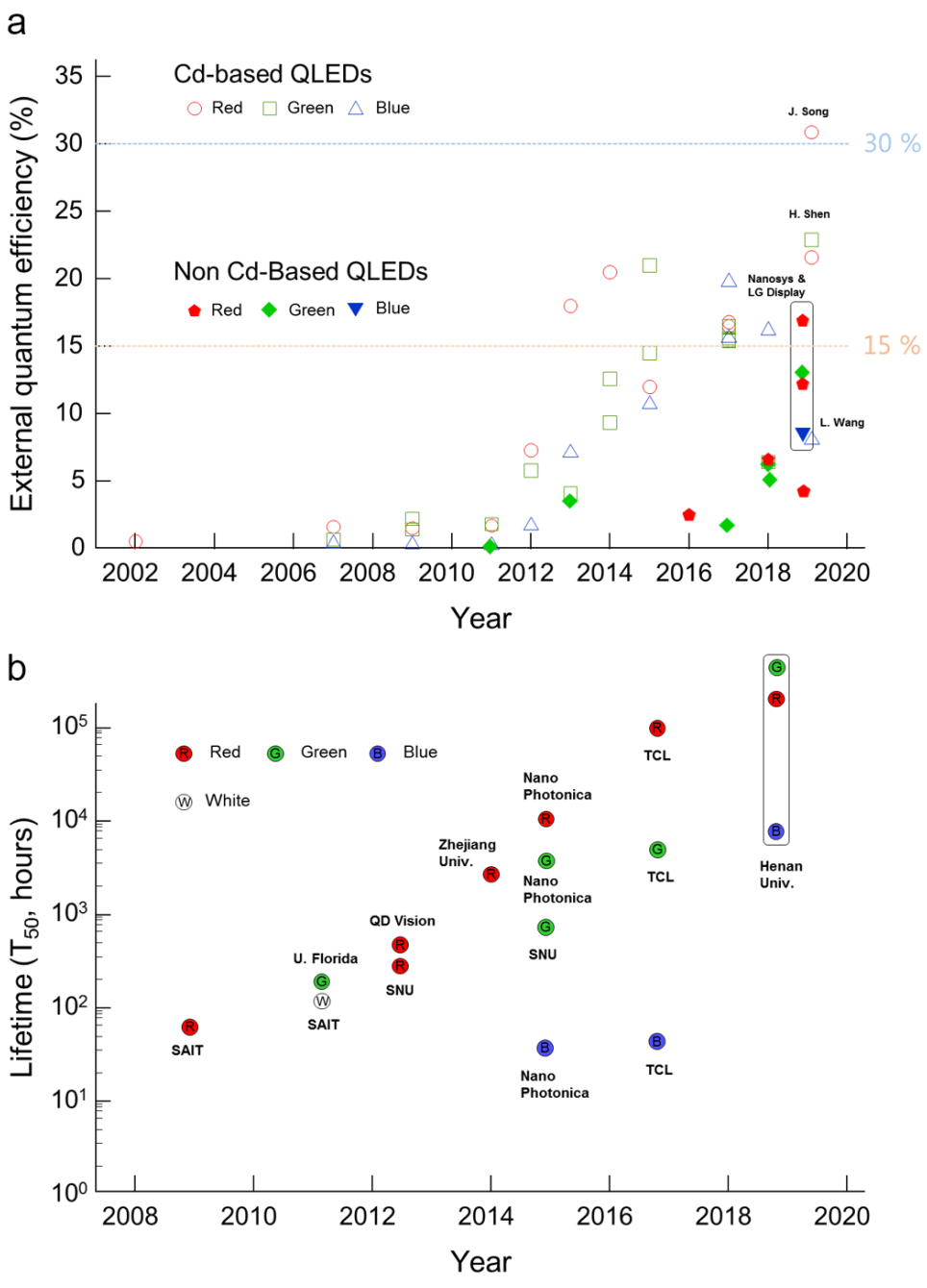

Figure 1.2 Progress in EQE and lifetime of QLEDs. The three primary colors, red (700-600 nm), green (600-500 nm), blue (500-400 nm) and white are categorized. [9, 30-33]

Currently, the main providers of QD technology for use in TVs are Nanosys and 3M, which provide the Quantum Dot film (QDEF) option for use with Full Array backlit LED/LCD TVs. The use QDs has taken big leap forward as several TV makers have shown off Quantum Dot-enabled TVs at tradeshows including Samsung, TCL, Hisense/Sharp, Vizio, and Philips. Samsung and Vizio have brought models to market in the U.S. QLED TVs are much more similar to traditional LED TVs: they have an LED backlight behind a layer of pixels that generates the picture. However, unlike traditional LED TVs, they use quantum dots as a filter to produce more accurate and better saturated colors. Furthermore, while their response time is very good, they don't suffer from the same stuttering that OLED TVs do. Their black levels are good for an LED TV and viewing angles are more akin to LED TVs as well.

While OLED is able to make screens much darker for better contrast, QLED display screens are a lot brighter. This makes it ideal for brighter rooms and content that are HDR. They also come in various sizes, big to small, and is also a lot affordable in comparison to OLEDs. To compare, Samsung's QLED TVs come in 43-inch to 98-inch sizes. This is an advantage as large televisions fastest-growing segment of the market, which makes Samsung the better option in this aspect. It also has the better outlook in being able to evolve further and better, as Samsung has revealed a version of QLED that does use emissive technology, much like OLED and plasma. Known as direct-view quantum dot, it dispenses with the liquid crystal layers and uses quantum dots themselves as the light source.

a

b

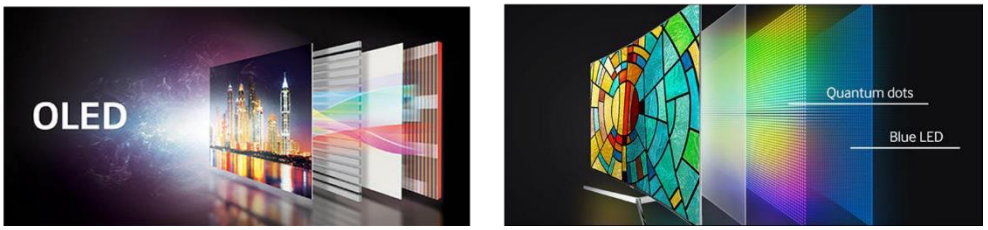

Figure 1.3 QLED and OLED (a) application on the premium TVs and (b) composition

(Pictures are referred to following websites: www.insidevina.com, www.stuff.tv)

1.2 Charge Balance Issues in QLEDs

QD-LEDs are expected to serve as a next-generation display technology, succeeding organic light-emitting diodes. However, there are several problems related to QD-LEDs, such as leakage current through QD surface states and insufficient charge injection into the QD cores, due to the energy barriers of QD shells; these charge injection imbalance result in exciton quenching and auger recombination, leading to degradation of device performance. As previously mentioned, the charge carrier injection balance is important for high-performance QD-LEDs. Metal oxides, such as ZnO, SnO_2 and zinc tin oxide (ZTO), have been used to fabricate electron transport layers (ETLs), which could improve electron injection into the QD emissive layer [34]. Inorganic compounds, such as metal oxides, have superior thermal stability and resistance against oxygen and moisture compared to organic compounds and have high mobility which can efficiently transfer electrode to QDs. Among the various metal-oxide ETL materials, solution-processed ZnO nanoparticles (NPs) provide superior QD-LED performance compared to other vacuum-deposited metal oxides. Inspired by the results of QD-LEDs with the ZnO NP ETL, there has been continuous research on solution-processed metal-oxide ETLs [35-37]. Nevertheless, the inverted QD-LEDs also face difficulties and challenges of charge-injection imbalance caused by the large potential energy barrier between QDs and hole transport layers (HTLs) as well as the carrier mobility difference between ETLs and HTLs. In particular, the electron injection from ETL to QDs is promoted due to a nearly barrier free transporting channel, whereas the hole injection from HTLs to QDs is much difficult, which is induced by a large energy barrier (0.6 eV or more). Moreover, the electron mobility of ETLs (ZnO, widely used) is higher than the hole mobility of HTLs [38-40]. Thereby, it is desirable for a hole transport material having high LUMO and low

HOMO energy level simultaneously, which can block the electron to diffuse into HTL and enhance the hole injection from HTL to QDs. In other words, a wide band gap hole transport material is necessary for efficient QD-LEDs. Various processes have been proposed to form the HTL, including phase separation [41], thermal polymerization, and evaporation [42]. However, how to design a highly efficient HTL structure is still a major challenge in the conventional QD-LEDs due to the limitation of solution technology, in which the underlying solvent-sensitive organic layers are inevitably damaged to a certain extent to achieve a multilayer device structure even though orthogonal solvents are used. In addition, most of the reported QD-LEDs suffer from unbalanced charge transport due to the misalignment between the extremely low valence band edge of QDs against the HOMOs of organic HTLs and lower hole mobility of polymer hole transport materials than that of ZnO nanoparticle ETL. For this reason, there are many reports in QD-LEDs aims for reducing charge injection imbalance [9, 23, 31, 32, 39, 43, 44].

Also, despite substantial progress made in the performance, the state-of-the-art QD-LEDs are still in need of operational stability that is a prerequisite factor for their practicable use. The origin of operational instability of QD-LEDs is unveiled to originate from the charge injection imbalance [45]. The disparity between charge carrier injection rates results in the accumulation of excess charge carriers within the QD emitters that promotes non-radiative Auger recombination processes [25, 46-48], leading to a reduction of luminance efficiency of QD-LEDs. In addition, the overflow of charge carriers across the QD emissive layer toward counter electrodes provokes degradation of charge transport layers [49-51] that causes irreversible degradation of QD-LEDs.

Equalized charge carrier injection rates promise a long-lived QD-LED [52-56]. The most widely attempted approach to reach the charge carrier balance is

decelerating the injection rate of dominant charge carriers. Inserting an electron blocking layer at the interface between the electron transport layers (ETL) and the QD emissive layer [27, 57-59] or lowering the carrier mobility of electron transport layers [60, 61] are the representative examples for the state-of-the-art QD-LEDs, in which the injection rate of electrons into QDs far exceeds that of hole. These negative incentives permit the increase in the device efficiency, but simultaneously accompany an unwanted outcome, the increase in the operation voltage to gain the fixed current density, that could accelerate degradation of the device by Joule heating. Therefore it is prerequisite to alleviate the charge injection imbalance not by reducing electron injection property ("Negative approach") but by enhancing hole injection property ("Positive approach") of QD-LEDs.

1.3 Outline of Thesis

This thesis consists of five chapters, including the Introduction and Conclusion. As an introduction, Chapter 1 describes the previous research on colloidal QD-LEDs and the key issues for improving efficiency and lifetime of QD-LED. Chapter 2 includes the methods for preparing materials: the methods used to prepare ZnO nanoparticles; the highly luminescent type I red heterostructured QDs; and the organic materials used in this thesis are described in detail. In addition, the fabrication and characterization methods for the QD-LED devices are summarized in this chapter, and the electrical and morphological characterization methods for thin films used in this thesis are depicted. Characterization methods for electrical and morphological characteristics of thin films are also described in this Chapter. In Chapter 3, the influence of hole injection interlayer (HIIL) with deep HOMO energy level on the performance of QD-LEDs is evaluated. The HIIL of Bis[2-(diphenylphosphino) phenyl] ether oxide (DPEPO), 1,4-Bis(triphenylsilyl)benzene (UGH-2), fullerene (C_{60}), Dipyrazino[2,3-f:2',3'-h]quinoxaline-2,3,6,7,10,11-hexacarbonitrile (HAT-CN) and 4,4´´-bis(triphenylsilanyl)-(1,1´,4´,1´´)-terphenyl (BST) are screened to investigate the efficiency and turn-on voltage of QD-LEDs. Then we found that when we use 4,4´-bis(N-carbazolyl)biphenyl (CBP) has HTL higher HOMO energy level of HIIL leads to the enhanced device performance. We choose C_{60} as the most optimized HIIL for QD-LEDs and analyzed the enhanced electrical property of hole only devices (HODs) and QD-LEDs by impedance spectroscopy and temperature experiment. The impedance spectroscopy result shows enhanced interlayer property between CBP (HTL) and MoO_x (HIL) due to the elimination of universal hole injection barrier by pinning effect of MoO_x. This enhanced interlayer property was reconfirmed by temperature experiment which we could obtain reduced activation

energy of HODs with thin C_{60} HIIL compared to that of HODs without thin C_{60} HIIL. Overall device performance (Turn-on voltage, leakage current, efficiency, luminance, and lifetime) was enhanced by reduced charge injection imbalance into QD emissive layer. Lifetime and operational stability of QD-LEDs with and without C_{60} HIIL is discussed in Chapter 4. By applying unique structure that comparing two architecture had almost similar but only difference with thin C_{60} HIIL which is suggested in previous Chapter, we quantitatively assessed operational stability of QD-LEDs. We isolated electroluminescence and photoluminescence of QDs and QD-LEDs and compared degradation factors in the devices. The impedance spectroscopy analysis of degraded QD-LEDs was conducted to confirm the HTL degradation effect and effect of joule heating was analyzed by temperature lifetime studies. Finally, in Chapter 5, we summarize our work and present concluding remarks.

Chapter 2

Experimental Methods

2.1 Materials

2.1.1 Preparation of ZnO Nanoparticles

ZnO nanoparticles were synthesized modifying the method reported by Pacholski *et al*.[62] At first, 1.23 g of $Zn(Ac)_2 \cdot 2H_2O$ was dissolved in 55 ml of methanol at room temperature. Then, 25 ml of a methanol solution containing 0.48 g of KOH was added dropwise at 60 ºC with magnetic stirring. The reaction mixture was kept at 60 ºC for 2 h under N_2 atmosphere. The product appeared as white precipitate. After collecting by centrifugation, this white precipitate was washed with methanol. Finally, 0.1 ml of butylamine was added for stabilization and the precipitate was redispersed in butanol (20 $mgml^{-1}$).

2.1.2 Synthesis of Red-color Emitting CdSe(core radius (r) = 2.0 nm)/$Zn_{1-X}Cd_XS$(shell thickness (h) = 6.0 nm) Core/shell Heterostructured Quantum Dots

Chemicals: Zinc acetate ($Zn(ac)_2$, 99.99%, metals basis), Oleic acid (OA, 90%), 1-octadecence (ODE, 90%), tri-n-octylphosphine (TOP, > 99%), sulfur (S, 99.998%, powder), and selenium (Se, 99.99%, pellet) were purchased from UniAm (Korea). Cadmium oxide (CdO, 99.95%, metals basis), myristic acid (MA, > 99%), and 1-dodecanethiol (DDT, >98%) were purchased from Alfa Aesar. All organic solvents were used as received from Daejung (Korea) without purification.

Synthesis of CdSe/$Zn_{1-X}Cd_XS$ QDs: QDs were synthesized same method reported by Kwak at el. and Bae at el..[5, 47] Synthesized QDs were purified 10 times by the precipitation/redispersion (ethanol/toluene) method. Final products were dispersed in hexane at a concentration of 20 $mgml^{-1}$. All chemistry was conducted under an inert condition (Ar) by using the Schlenk line technique. We prepared stock solutions (0.5 M $Cd(OA)_2$ and $Zn(OA)_2$ diluted with ODE for cation precursors, and 2 M TOPSe and TOPS for anion precursors) and used them for QD synthesis. For CdSe core (radius = 2 nm) synthesis, 1 mmol of CdO, 3 mmol of myristic acid (MA) and 15 mL of ODE were stirred and degassed at 110 ^oC for an hour. After back-filled with Ar, the reaction flask was heated to 300 ^oC. At the elevated temperature, 0.25 mL of 2 M TOPSe was rapidly injected into the reaction flask to initiate CdSe nucleation. After 3 min of reaction, 3 mL of $Zn(OA)_2$ precursor and 1 mmol of 1-dodecanethiol (DDT) were added to grow the first $Zn_xCd_{1-x}S$ shell. After 30 min of reaction, 2 mL of

$Cd(OA)_2$ precursor, 4 mL of $Zn(OA)_2$ precursor and 1.5 mL of 2 M TOPS were additionally injected in a minute for second $Zn_xCd_{1-x}S$ shell growth. This step is repeated for 4times. After 10 min of reaction, the reaction flask was cooled down to room temperature to complete the reaction. Synthesized QDs were purified repeatedly via precipitation (acetone) and redispersion (toluene) method. Final products were dispersed in toluene (15 mg/ml) and kept in a refrigerator for device fabrication.

2.1.3 Organic Materials

4,4'-bis(carbazol-9-yl)biphenyl (CBP), Bis[2-(diphenylphosphino) phenyl] ether oxide (DPEPO), 1,4-Bis(triphenylsilyl)benzene (UGH-2), fullerene (C_{60}), Dipyrazino[2,3-f:2',3'-h]quinoxaline-2,3,6,7,10,11-hexacarbonitrile (HAT-CN) and 4,4´´-bis(triphenylsilanyl)-(1,1´,4´,1´´)-terphenyl (BST) are purchased from OSM as hole injection interlayer. Chemical structures of organic materials used in this thesis are as follows.

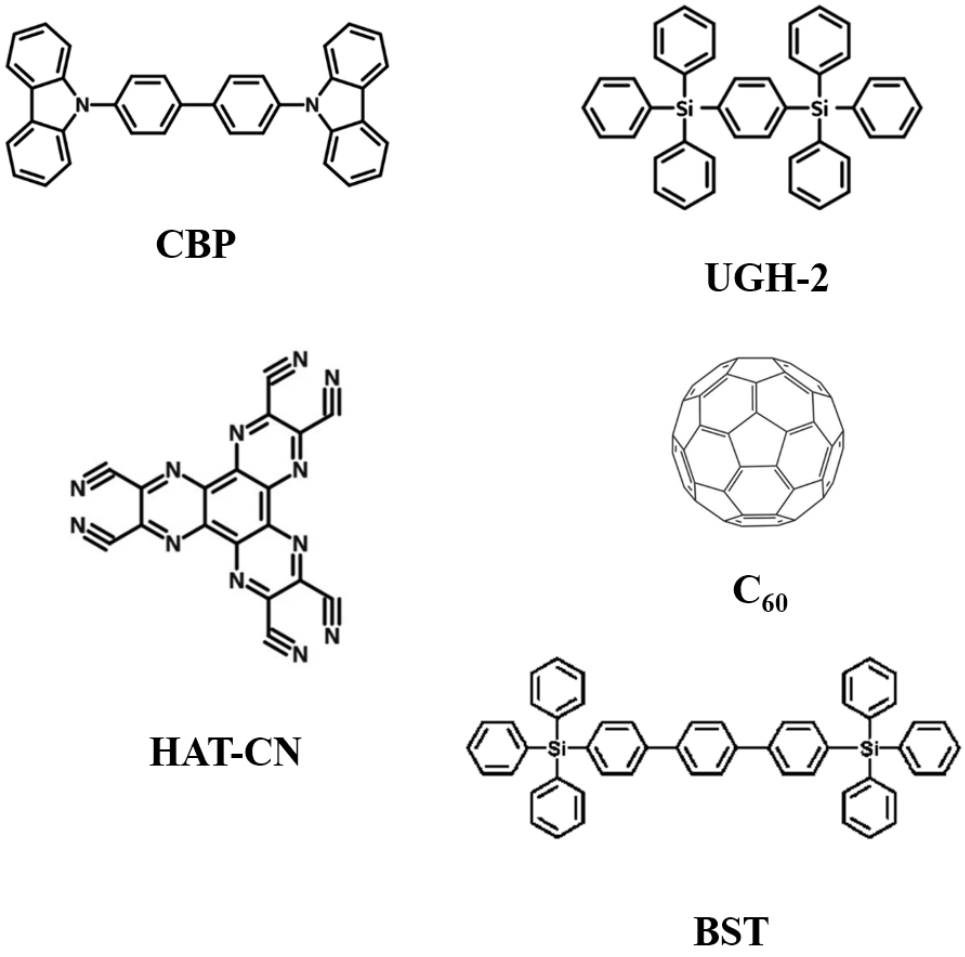

Figure 2.1 Chemical structures of CBP, UGH-2, HAT-CN, C_{60} and BST.

2.2 Device Fabrication and Characterization Methods

2.2.1 Device Fabrication

All QD-LED devices were basically fabricated using the inverted structures and the detail structures, materials and processes are introduced in each chapter. First of all, patterned ITO glass substrates were prepared, which were cleaned with acetone, isopropanol and deionized water in an ultrasonicator (Branson 5510). And then the cleaned ITO glass substrates were dried in the oven at 120 ℃. For the inverted structure, 20 mg/mL of the ZnO nanoparticle solution was spin-coated on a patterned ITO glass with a spin-rate of 2000 rpm for 60 sec and dried at 90 ℃ for 30 min in the oven filled with N_2 gas. The thickness of ZnO layer as electron injection/transport layer was about 40 nm. QD solution was spun on the bottom layer at 4000 rpm for 30 sec, followed by baking in N_2 oven at a temperature of 70 ℃. Then HTLs CBP, HIIL (UGH-2, HAT-CN, C60 and BST), MoO_x, and Al electrode were thermally evaporated under a vapor pressure of 1×10^{-6} torr onto QDs coated substrates. The deposition rates of each layers were 1 $Å s^{-1}$ for CBP, UGH-2, HAT-CN, C60 and BST sole layer. And then MoO_x, and Al were thermally evaporated with rate of 0.2 $Å s^{-1}$, and 4–5 $Å s^{-1}$, respectively.

2.2.2 Current-voltage-luminance Measurement

The current-voltage (I-V) characteristics were measured with a Keithley 236 source measurement unit, while the electroluminescence was measured with a calibrated Si photodiode (Hamamatsu, S5227-1010BQ) with a size of 10 mm × 10 mm placed at an angle normal to the device surface, assuming that the device was a Lambertian source. To detect a turn-on voltage of light-emitting diodes, we use an ARC PD438 photomultiplier tube (PMT) with the Keithley 236 source measurement unit. The electroluminescence (EL) spectra and the Commission Internationale de L'Eclairage (CIE) color coordinates were measured with a Konica-Minolta CS-1000A spectroradiometer. The luminance and efficiency were calculated from the photocurrent signal of photodiode with a Keithley 2000 multimeter, and corrected precisely with the luminance from spectroradiometer (CS-2000).

The chromatic characteristics were calculated from EL spectra measured by the CS-1000A spectrometer using the CIE 1931 color expression system. The tristimulus values XYZ can be calculated by following equations,

$$X = K_m \int_0^\infty \bar{x}(\lambda) P(\lambda) d\lambda \tag{2.1}$$

$$Y = K_m \int_0^\infty \bar{y}(\lambda) P(\lambda) d\lambda \tag{2.2}$$

$$Z = K_m \int_0^\infty \bar{z}(\lambda) P(\lambda) d\lambda \tag{2.3}$$

where, P(λ) is a given spectral power distribution of emissive source, $\bar{x}$, $\bar{y}$ and $\bar{z}$ are the CIE standard color matching functions (see Figure 2.2) and Km is the weighing constant (683 lm W^{-1}). From the tristimulus values, the CIE color coordinates calculated by following equations,

$$x = \frac{X}{X+Y+Z} \tag{2.4}$$

$$y = \frac{Y}{X+Y+Z} \tag{2.5}$$

$$z = \frac{Z}{X+Y+Z} \tag{2.6}$$

Any color can be plotted on the CIE chromaticity diagram.

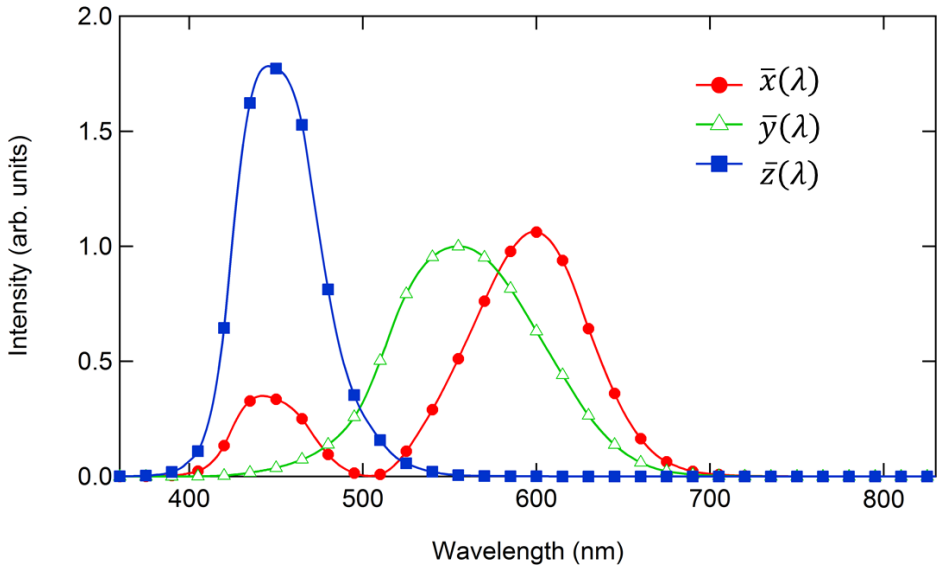

Figure 2.2 The CIE standard observer color matching functions

2.2.3 Efficiency Calculation Methods

To evaluate the emission properties of light-emitting diodes, the commonly employed efficiencies are the EQE, the current efficiency (C.E.) and the power efficiency (P.E.).

The external quantum efficiency can be defined by the following equation.

$$\mathrm{EQE} = \frac{number\ \ of\ \ emitted\ \ photons}{number\ \ of\ \ injected\ \ electrons}(\%)$$

Typically, QLEDs or OLEDs emit light into the half plane due to the metal contact. Without any modification for increasing out-coupling efficiency, over 80% of the emission can be lost to internal absorption and wave-guiding in a simple planar light-emitting device.

Since human eye has different spectral sensitivity in visible area, the response of the eye is standardized by the CIE in 1924 (see $\bar{y}$ in Figure 2.2). The luminous efficiency weighs all emitted photons according to the photopic response of human eye. The difference is that EQE. weighs all emitted photons equally. C.E. can be expressed by the following equation.

$$\mathrm{C.E.} = \frac{luminance}{current\ \ density}(cd\ \ A^{-1})$$

The luminance value (cd m^{-2}) can be easily measured by the commercial luminance meter (CS-1000A in this thesis).

The power efficiency is the ratio of the lumen output to the input electrical power as follows,

$$\mathrm{P.E.} = \frac{luminous\ \ flux}{electrical\ \ power}(lm\ \ W^{-1})$$

The EQEs can be useful to understand the fundamental physics for light emission mechanism, while the PEs can be useful to interpret the power dissipated in a light-emitting device when used in a display application.

2.2.4 Measurement of Electrical Characteristics

Device fabrication and characterization of hole only device (HOD): HOD with CBP HTL and thin C_{60} HIIL were fabricated and characterized to analyze enhanced electrical property of interface between CBP and MoO_x. Indium tin oxide (ITO) patterned glass was cleaned with acetone, isopropyl alcohol, and deionized water sequentially and then used as substrate for HOD. The prepared Poly(3,4'-ethylenedioxythiophene)-poly(styrenesulfonate) (PEODT:PSS) solution was spun-cast on patterned ITO substrates with a spin rate of 4000 rpm for 60 s. PEDOT:PSS films were then annealed at 120 °C under 100 mtorr pressure for 30 min. Then HTLs CBP, HIILs (UGH-2, HAT-CN, C60 and BST) , MoO_x, and Al electrode were thermally evaporated under a vapor pressure of 1×10^{-6} torr. Impedance spectroscopy were measured within the frequency range of 1 Hz to 1 MHz at an oscillation amplitude of 10 mV with varying DC bias voltages. The frequency dependent measurements were performed with impedance analyzer (Wayne Kerr 6500B). The relationship

$$\sigma = p \times e \times \mu,$$

relating conductivity (σ), mobility (μ), and carrier density is used to calculate the hole density (p), where e is 1.602×10^{-19}C.

2.2.5 Modeling and Simulation

Time-Correlated Single Photon Counting (TCSPC) measurement: The fabricated QD-LEDs were taken TCSPC measurement to analyze photo characteristics of devices. The absolute PL QY of the QD emissive layer before operation (t = 0) was measured with the PL measurement system coupled with the integrating sphere. The time-dependent PL QYs of the QD emissive layer were estimated by comparing PL intensities of the QD emissive layer that were measured under unbiased condition (applying voltage = 0) after device operation with the initial PL intensity. We note that the PL intensity and PL decay dynamics of the QD emissive layer remain constant during the ex situ measurements (~ 3 min).

Optical Characterization: UV−vis absorption and photoluminescence spectra were obtained with a Lambda 35 spectrometer (PerkinElmer) and a Fluoromax-4 spectrometer (Horiba Science), respectively. The absolute PL QYs of film samples were obtained at an excitation wavelength of 520 nm with a C11347-01 (Hamamatsu Photonics). The measurements to characterize the PL decay dynamics were conducted with a TCSPC system from Horiba-Jovin Yvon, which has a resolution of about 100 ps. The samples were excited at 2.38 eV at a repetition rate of 200 kHz.

Modeling and Simulation: The fraction of charged QDs and the electronic injection rate at a given time are assessed by taking into account the Coulombic interactions between the charge carrier within the QD emissive layer and the charge carrier in charge transport layers. The lowest quantized electronic states of QDs are calculated by performing the quantum mechanical calculation including self-consistency and dielectric mismatch effect in three dimension.

Modeling and Simulation: The fraction of negatively charged QDs and the electron injection rate at a given time ($\boldsymbol{J(t)}$) under constant current density ($\boldsymbol{J_h}$ = constant) can be obtained by considering coupled rate equations.

$$J_e(t) - J_h = \frac{dC(t)}{dt}$$

$$J_e(t) = J_e(0)(1 - \alpha \frac{C(t)}{N})$$

where $J_e(t)$ and J_h is the number of injected electrons and holes into QDs in unit area (cm^2) at time t, N is the number of QDs in unit area (cm^2), C(t) is the number of charged QDs in unit area (cm^2) at time t, and α is the repulsion coefficient for electron injection from ZnO ETL into negatively charged QDs.

From these equations, we can get the fraction of charged QDs and the electron injection rate at a given time ($J_e(t)$).

$$F(t) = \frac{C(t)}{N} = \frac{J_e(0) - J_h}{J_e(0)}(1 - \exp\left(-\frac{J_e(0)\alpha}{N}t\right))$$

$$J_e(t) = J_e(0) - (J_e(0) - J_h)(1 - \exp\left(-\frac{J_e(0)\alpha}{N}t\right))$$

2.2.6 Other Characterization Methods

UV-Visible Spectroscopy: The transmission and absorption spectra were measured with DU-70 UV/Vis Scanning Spectrophotometer (Beckman Coulter, Inc.) or Agilent 8454 UV-Vis. diode array spectrometer. In case of solution, materials were dissolved in toluene or chlorobenzene. For the film measurement, materials were spin-coated or evaporated thermally in the thickness of ~50 nm on quartz substrate. The reflectance spectra were measured by a Varian Cary 5000 spectrophotometer. The average transmittance (T_{avg}) was calculated by the following equation.

$$T_{\mathrm{avg}} = \frac{\int_{\lambda_1}^{\lambda_2} T(\lambda)\mathrm{d}\lambda}{\lambda_2 - \lambda_1} \tag{2.7}$$

Where $T(\lambda)$ is the transmittance as a function of the wavelength, T_{avg} was usually calculated by integrating $T(\lambda)$ from 400 nm (λ_1) to 800 nm (λ_2).

Ultraviolet Photoelectron Spectroscopy (UPS): The UPS spectra were performed using Kratos AXIS-NOVA, employing He I light source and a hemispherical analyzer. The valence band maximum (VBM) of the nanocrystals was calculated using the following equation.

$$VBM = 21.2\ eV - \left|E_{cutoff} - E_{onset}\right| \tag{2.8}$$

The conduction band minimum (CBM) value was obtained by using the VBM and the excitonic band gaps of QDs, estimated from the PL spectra of QDs.

Film Thickness Measurement: Ellipsometers (L2W15S830 with 632.8-nm He-Ne laser light, Gaertner Scientific Corp. and M2000D, Woollam) and an AFM (XE-100, Park Systems) were used for measuring the thicknesses of films

Transmission electron microscopy (TEM): The TEM images of the QDs were obtained using a Tecnai TF30 ST at 200 KV to analyze their average size and size distribution. The energy dispersive x-ray (EDX) spectra of QDs were acquired through Si-Li detector of Oxford INCA Energy attached on main body of TEM. Low-coverage samples were prepared by placing a drop of a dilute toluene dispersion of QDs on a copper grid (300 mesh) coated with an amorphous carbon film. The composition of QDs was measured with inductively coupled plasma optical emission spectroscopy (Agilent ICP-OES 720).

QDs' general characterization: A photoluminescence quantum yield (PL QY) was acquired in the comparison of their fluorescence intensities with those of primary standard dye solution (coumarin 545, quantum yield = 95 % in ethanol) at the same optical density (below 0.05) at same excitation wavelength (400 nm). For photoluminescence lifetime measurements, the samples were excited at 488nm (pulse width ~ 40 ps) at a repetition rate of 2 MHz. PL dynamics were measured using time-correlated single-photon counting (TCSPC) system that consists of avalanche photodiodes (timing resolution ~ 350 ps) and a multi-channel analyzer (Picoquant Hydraharp).

Chapter 3

Modification of Hole Transport Layer for Efficient and Stable Quantum Dot Light-Emitting Diodes

Colloidal quantum dot light-emitting diodes (QD-LEDs) are p-i-n junction diodes exhibiting excellence in color gamut, brightness and flexible form factors, promising their use in next-generation displays.[1-3, 5] Within the last few decades, QD-LEDs have demonstrated great progress in efficiency and brightness that are comparable to the performance of commercialized organic light-emitting diodes (OD-LEDs) are reported.

To enhance performance of QLEDs, lots of attempts have been made on QD and QD-LED, such as modifying core/shell composition and structure, surface ligand

modification, and optimization QLEDs device architectures. [52, 63] Through these methods, tremendous improvement in terms of photoluminescence quantum yields (PL QY) of QDs and EQE of QD-LEDs have been accomplished. However, there are several problems related to QD-LEDs, such as leakage current through QD surface states and insufficient charge injection into the QD cores, due to the energy barriers of QD shells; these charge injection imbalance result in exciton quenching and auger recombination, leading to degradation of device performance. the inverted QD-LEDs also face difficulties and challenges of charge-injection imbalance caused by the large potential energy barrier between QDs and hole transport layers (HTLs) as well as the carrier mobility difference between ETLs and HTLs. In particular, the electron injection from ETL to QDs is promoted due to a nearly barrier free transporting channel, whereas the hole injection from HTLs to QDs is much difficult, which is induced by a large energy barrier (0.6 eV or more). One way to alleviate charge imbalance is reducing electron injection property by reducing electron mobility of ETL or inserting electron blocking layer (EBL) between ETL and QD EML [4, 52, 60, 64]. However this "Negative approach" of balancing charge injection result in increasing operational condition of QD-LEDs which is critical for stable operating devices. Therefore it is important to enhance hole injection property of QD-LEDs ("Positive approach") for high efficient and stable devices.

In this study, we demonstrated improved QD-LEDs lifetime and performance with enhanced hole transport property by insertion of thin fullerene (C_{60}) as hole injection interlayer between CBP HTL and MoO_x layer. Insertion of buffer layer which has high highest occupied molecular orbital (HOMO) level such as C_{60} can eliminate pinning effect between CBP and MoO_x layer. This eventually increase hole transport property in QD-LEDs and enhance balance of electron and hole transport rate to QD emissive layer.

As a result, the QD-LEDs with C_{60} interlayer showed 10% reduced initial rapid luminance drop compared to non- C_{60} interlayer QD-LEDs which leads to 5 times increase in operational lifetime at 1000 nit. (75 % lifetime (LT_{75}) ~ 5.6 hours @ 1000 cd/m^2 for non-C_{60} interlayer QLEDs and (LT_{75}) ~ 36.5 hours @ 1000 cd/m^2 for C_{60} interlayer QD-LEDs).

3.1 QDs based LEDs made of a Series of HIIL with Deep HOMO Energy Levels

We have synthesized CdSe/$Zn_xCd_{1-x}S$ core/shell heterostructured QDs for emissive material of QD-LEDs. Synthesized QD is composed of core radius = 2.0 nm and shell thickness = 5.5 nm and stabilized with oleic acids that allow QDs dispersed in toluene solvent and preserve aggregation of QDs. Transmission electron microscopy (TEM) image of QDs shows the uniform distribution of synthesized QDs and photoluminescence (PL) spectra of CdSe/$Zn_xCd_{1-x}S$ core/shell heterostructured QDs is centered at 640 nm. Injected charge carrier imbalance within QD emissive layer cause non-radiative Auger recombination process. To alleviate charge injection imbalance, we inserted deep HOMO level material between CBP and MoO_x to increase hole injection property of QD-LEDs. To figure out relation between HOMO energy level of HTL and the device characteristics of QD-LEDs, we screen the commercially available deep HOMO energy level material range over 6.0 eV, which is the HOMO level of CBP. Bis[2-(diphenylphosphino) phenyl] ether oxide (DPEPO) [65, 66], 1,4-Bis(triphenylsilyl)benzene (UGH-2) [67, 68], fullerene (C_{60}) [69, 70], Dipyrazino[2,3-f:2',3'-h]quinoxaline-2,3,6,7,10,11-hexacarbonitrile (HAT-CN) [71, 72] and 4,4´´-bis(triphenylsilanyl)-(1,1´,4´,1´´)-terphenyl (BST) [67, 73] are treated as HIIL of QD-LED.

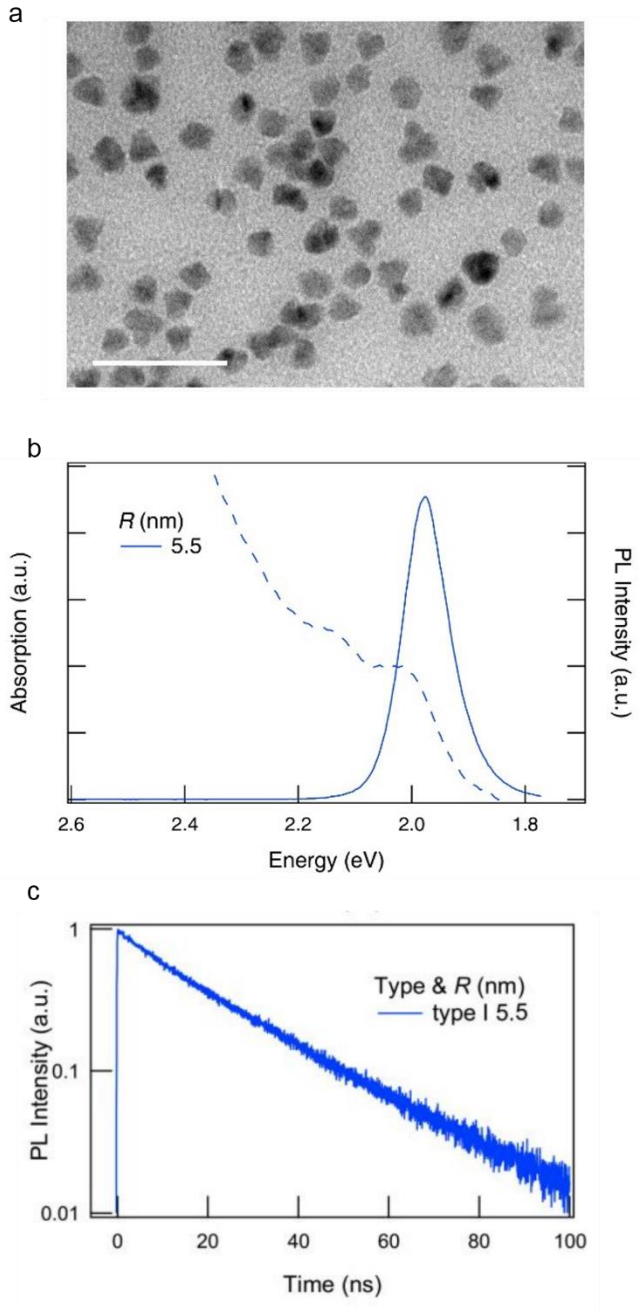

Figure 3.1 (a) Transmission electron microscopy (TEM) images and (b) absorbance and photoluminescence spectra of CdSe (r = 2 nm)/ $Zn_xCd_{1-x}S$ (h = 5.6 nm) type 1 red QDs. (c) solution PL decay curve [74]

Table 3.1 HOMO energy level characteristics of hole injection interlayers (HIIL).

	HOMO (eV)	**LUMO (eV)**	**Reference**
HAT-CN	9.7	5.8	70, 71
DPEPO	6.8	2.6	64, 65
UGH-2	7.2	2.8	66, 67
C_{60}	6.4	3.7	68, 69
BST	6.25	2.5	66, 72

3.2 Characteristics of Electroluminescence Devices with various HIIL.

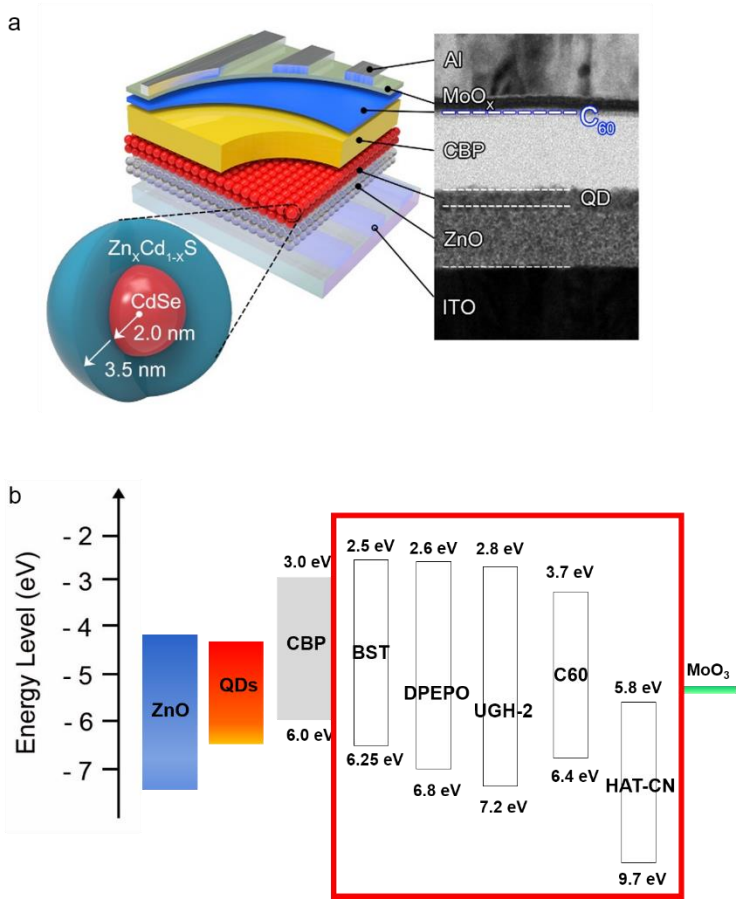

Figure 3.2 (a) Schematic illustration (left) and cross-sectional transmission electron microscopy (TEM) image (right) of red QD-LEDs with HIIL and architecture of type 1 11 nm diameter red QDs (bottom).[74] (b) Energy level diagram of QD-LEDs employing BST, DPEPO, UGH-2, C_{60} and HAT-CN as HIIL.

Figure 3.2a shows the inverted structure of QD-LEDs in a configuration of ITO//ZnO//QDs//CBP//HIIL//MoOx//Al. BST, DPEPO, UGH-2, C60 and HAT-CN are chosen to their deep HOMO energy level compared to CBP (6 eV). Energy level

of each layer is illustrated in Figure 3.2b. The device characteristics of QD-LEDs using BST, HAT-CN, and C_{60} as HIIL is displayed in Figure3.3 ~ Figure3.6. The devices with various BST HIIL showed maximum EQEs of each 5.2 %, 5.3 %, 5.2 %, 5.0 % and 5.0 % for thickness of 0, 1, 3, 5, and 7 nm respectively. (Figure 3.3) The EQE of device is increased with the thin layer of BST HIIL and more importantly the EQE of low current density region largely increased. The driving voltage (operation voltage of device at the brightness of 100 cdm^{-2}) of each device is 4.4 V, 4.3 V, 4.1 V, 4.2 V, and 4.5 V for thickness of 0, 1, 3, 5, and 7 nm respectively. The driving voltage of device is reduced as the insertion of BST HIIL. This result means that the insertion of BST HIIL enhances hole injection property of QD-LEDs due to eliminating energetic barrier between CBP HTL and MoO_x HIL by pinning effect of MoO_x [75-77]. The approach simply involves an insertion of a thin interlayer, which has higher ionization energy (IE) than an organic HTL, between the metal oxide and an organic HTL. Along with its easy applicability to QD-LEDs employing hybrid CTLs without altering either the device configuration or the CTL materials, the approach enables to individually control the hole injection current. The barrier reduction is accomplished by electrostatic decoupling of the MoO_x from the organic hole transport material with an insertion of deep HOMO energy level thin interlayer. This interlayer highly alleviate the effect of the attractive image potential near the MoO_x interface which reduces the pinning effect, and eliminates the DOS broadening present at the HTL/MoO_x interface, while restoring Fermi-level alignment. Less effective but similar characteristics also can be seen HIIL with HAT-CN HIIL. (Figure 3.4) Although the devices with 3 nm HAT-CN HIIL showed reduced maximum EQEs from 5.0 % (pristine QD-LEDs) to 4.9 % (with 3 nm HAT-CN HIIL QD-LEDs), the EQE of low current density region increased. The driving voltage reduced as same as BST HIIL from 4.1 V (pristine QD-LEDs) to 3.9 V (with 3 nm HAT-CN HIIL QD-

LEDs). Most of all, the insertion of C_{60} HIIL showed most effective enhancement on electroluminescence characteristics of QD-LEDs. (Figure 3.5) For the specific analysis of enhancement on electrical and optical property of QD-LEDs, we choose C_{60} as HIIL layer and conducted various analysis.

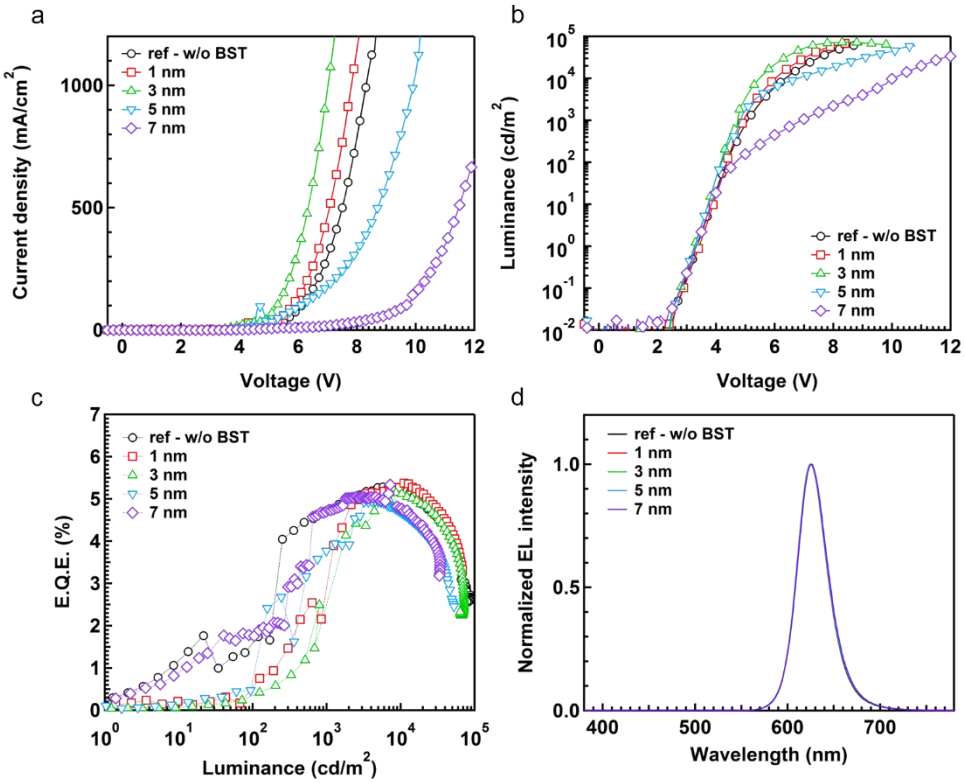

Figure 3.3 EL characteristics (a) Current density-voltage (b) voltage-luminance curves and (c) current density dependent device efficiencies (EQE) (d) Normalized EL intensity of QD-LEDs with controlling the thickness of BST thin layer (1, 3, 5, and 7 nm).

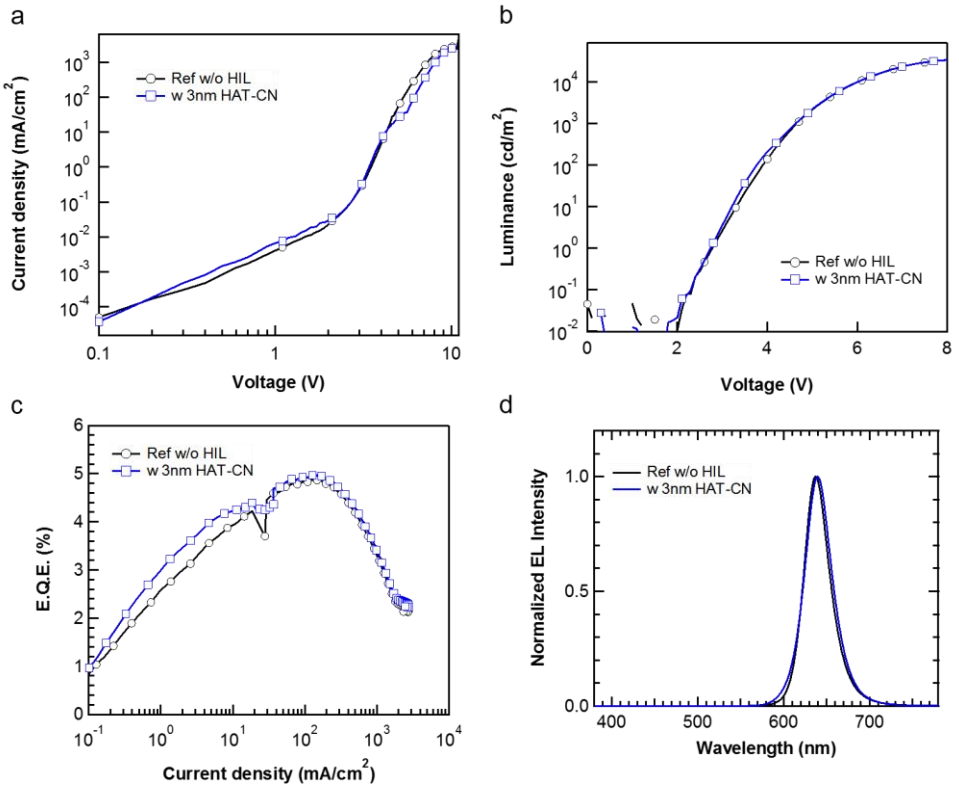

Figure 3.2 EL characteristics (a) Current density-voltage (b) voltage-luminance curves and (c) current density dependent device efficiencies (EQE) (d) Normalized EL intensity of QD-LEDs with and without 3 nm of HAT-CN HIIL.

Table 3.2 EL characteristics of QD-LEDs with controlling the thickness of BST HIIL.

	Driving voltage @ 100 cd/m^2 [V]	**Peak EQE [%]**
w/o	4.4	5.2
1 nm	4.3	5.3
3 nm	4.1	5.2
5 nm	4.2	5.0
7 nm	4.5	5.0

Table 3.3 EL characteristics of QD-LEDs with HAT-CN HIIL.

	Driving voltage @ 100 cd/m^2 [V]	**Peak EQE [%]**
w/o	4.1	5.0
3 nm	3.9	4.9

The state-of-the-art QD-LED with a record efficiency employs hybrid charge transport layers (CTLs, inorganic ETL and organic hole transport layer (HTL)) that deliver charge carriers from electrodes toward the QD emissive layer (Figure 3.6a) [78]. For a QD-LED showing an internal quantum efficiency (IQE) close to the photoluminescence quantum yield (PL QY) of the QD emissive layer, the disparity between electron versus hole injection rates into QDs is calculated to be insignificant (here, $[J_e(0) - J_h(0)]/J_e(0) \cong 6.5\times10^{-9}$). This promises that the increase in the hole current will certainly achieve the charge injection balance in QD-LEDs and thus enhance the operational stability of devices. We modulate the hole current density by controlling the thickness of C_{60} HIIL and characterize their influence on the device performance. As a test bed, we adopt inverted QD-LEDs that employ ZnO nanoparticles and 4,4'-bis(9-carbazolyl)-1,1'-biphenyl (CBP) as ETL and HTL, respectively. CdSe (radius = 2.0 nm)/$Zn_XCd_{1-X}S$ (shell thickness = 3.5 nm) type I core/shell heterostructured QDs, whose photophysical properties are well understood, are chosen as the emissive materials. The reference QD-LED (without an interlayer) shows peak EQE of 6.7 % at the current density (J) of 25 mA/cm^2 (applied voltage (V) = 3.6 V). Considering PL QY of the QD emissive layer (43 %) and the out-coupling efficiency (η_{out}) of current devices (20 %), the insertion of C_{60} interlayer enhance the device efficiency close to the theoretical limit (~ 8.6 %). We insert fullerene (C_{60}, IE = 6.4 eV) layers of varying thicknesses (i.e., 0, 2, 3 and 5 nm) at the interface between HTL and MoO_X hole injection layer (HIL).

The insertion of C_{60} interlayer helps suppress the leakage current below the threshold voltage (< 2.0 eV), indicating that the interlayer plays as the tunneling barrier for hole leakage from MoO_X toward CBP. The trend in the current density of QD-LEDs above the threshold varies significantly depending on the thickness of C_{60} interlayer. Specifically, 3 nm thick C_{60} interlayer enhances the current density of

devices at most by a factor of 8 at the applied voltage of 4 V, whereas 5 nm thick C_{60} interlayer reduces the current density by 30 % at the same applied voltage. QD-LEDs with 2, 3 nm thick C_{60} interlayer exhibit enhanced luminescence efficiency at the current density below 200 mA/cm^2, suggesting that electron-hole injection imbalance into the QD emissive layer is mitigated at the low current density (applied voltage) regime. As a combined result of the reduction in the operation voltage and the enhancement of the charge injection balance, QD-LEDs having 2, 3 nm thick C_{60} interlayer show significant improvement of power efficiency at the low current density (applied voltage) regime.

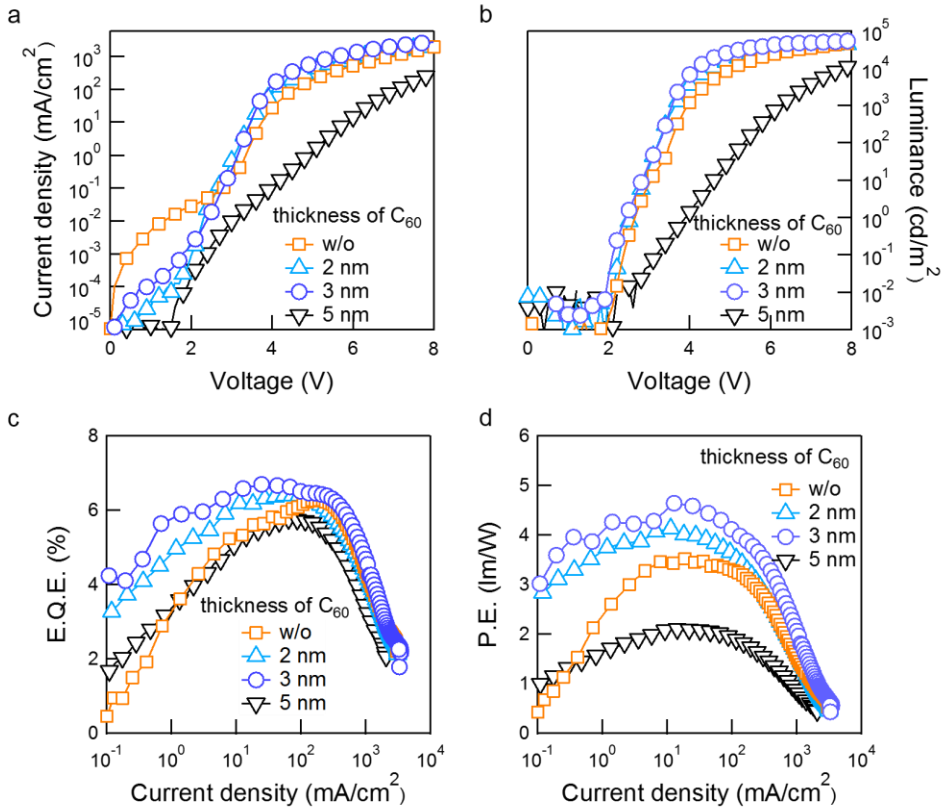

Figure 3.5 EL characteristics (a) Current density-voltage (b) voltage-luminance curves and (c) current density dependent device efficiencies (EQE) (d) and current density dependent device power efficiency (PE) of QD-LEDs with controlling the thickness of thin C_{60} HIIL (2, 3, and 5 nm).[74]

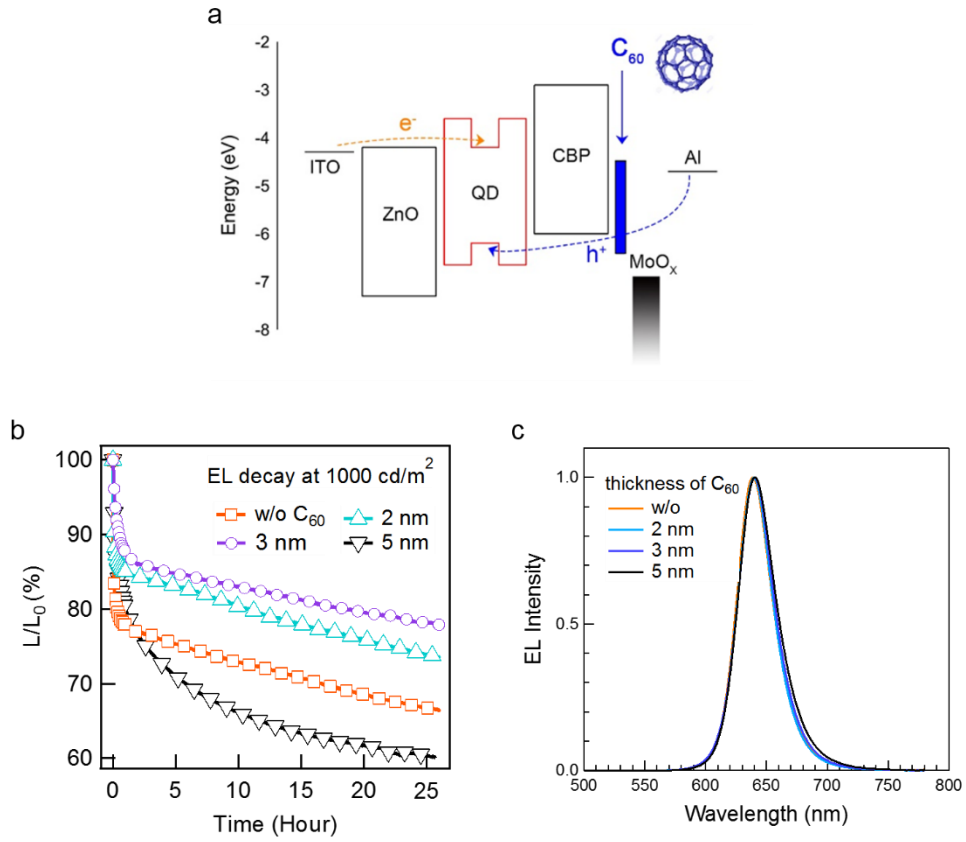

Figure 3.6 (a) Device architecture and schematic illustration of enhanced hole injection property in QD-LEDs with thin C_{60} HIIL (b) Lifetime characteristics and (c) Normalized EL Intensity of QD-LEDs with controlling the thickness of thin C_{60} HIIL (2, 3, and 5 nm).[74]

Table 3.4 EL characteristics of QD-LEDs with controlling the thickness of C_{60} HIIL.

	Driving voltage @ 100 cd/m^2 [V]	**Turn on Voltage @ 1 cd/m^2 [V]**	**Peak EQE [%]**	**Peak PE [%]**
w/o	3.5	2.7	6.2	3.5
2 nm	3.2	2.5	6.4	4.1
3 nm	3.2	2.4	6.7	4.6
5 nm	5.3	3.9	5.8	2.6

3.3 Electrical Characteristics of HODs with HIIL analyzed by Impedance Spectroscopy

The notable changes in the current density are apparently attributed to the variation of the hole current by the insertion of C_{60} interlayer. To identify changes in the hole current from cathode to HTL, we fabricate hole-only-devices (HODs) with varying C_{60} interlayer thicknesses and assess their electrical properties (Figure 3.7a,b). HODs are constructed in an architecture of ITO (150 nm)//PEDOT:PSS (40 nm)//CBP (60 nm)//C_{60} interlayer (thickness = 0, 2, 3 or 5 nm)//MoO_X (10 nm)//Al (130 nm). The cole-cole plots in impedance spectroscopy (IS) analysis on HODs (Figure 3.10 a~c) and full devices (Figure 3.10 d~f) show significant reduction of device resistance with the insertion of 2, 3 nm thick C_{60} interlayer, indicating that the employment of C_{60} interlayer reduces the resistance at the interface between CBP and MoO_X//Al. The hole current rises at most by factor of 8 with the insertion of 3 nm thick C_{60} interlayer, but decreases when 5 nm thick C_{60} interlayer is implanted. Electrical characteristics of devices and impedance spectroscopy coherently attest that insertion of 2, 3 nm C_{60} interlayer enables Ohmic contact between MoO_X toward CBP by eliminating the universal hole blocking barrier existing at the interface and facilitates the hole supply to the QD emissive layer. Simultaneously, the C_{60} interlayer plays as the tunnel barrier for hole injection, and thus the increase in the interlayer above the critical thickness (here, 3 nm) in turn gives rise to the reduction of hole currents and deteriorates the device efficiency.

Eliminating the universal hole blocking barrier at the interface between CBP and MoO_X//Al increases the device efficiency substantially at the lower current density regime ($J < 50$ mA/cm^2). The increment in the device efficiency by the implanted interlayer diminishes at higher current density regime and eventually the impact

vanishes at the current density above 200 mA/cm^2. Regardless of the current density or the device efficiency, the insertion of C_{60} interlayer alters the operation voltage to reach the fixed current density. Therefore, comparative analysis among QD-LEDs with varying interlayer thicknesses both at the low current regime (J = 30 mA/cm^2, L = 1,000-2000 cd/m^2) and the high current density regime (J = 200 mA/cm^2, L = 10,000 cd/m^2) enables us to understand the impact of the device characteristics (e.g., charge injection imbalance, operation voltage) on the operational stability of QD-LEDs.

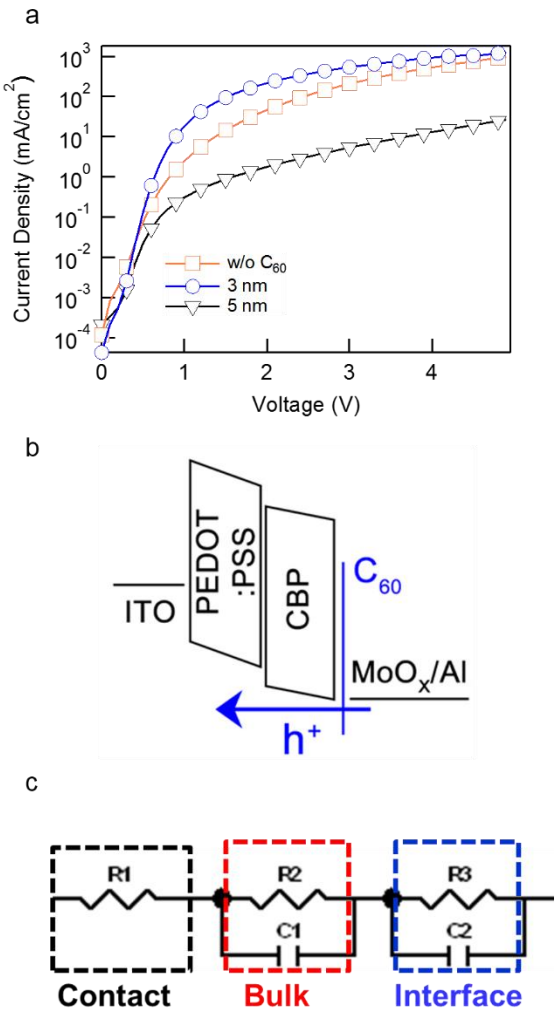

Figure 3.7 (a) Current density-voltage characteristics of HODs employing varying thicknesses of C_{60} interlayer. An inset depicts the HOD structure.[74] (b) Schematic illustration of hole injection enhancement mechanism by insertion of C_{60} HIIL in HODs (c) Equivalent circuit composed of contact resistance, bulk component, and interface component for fitting the cole-cole plot of HODs with various thickness of C_{60} HIIL.

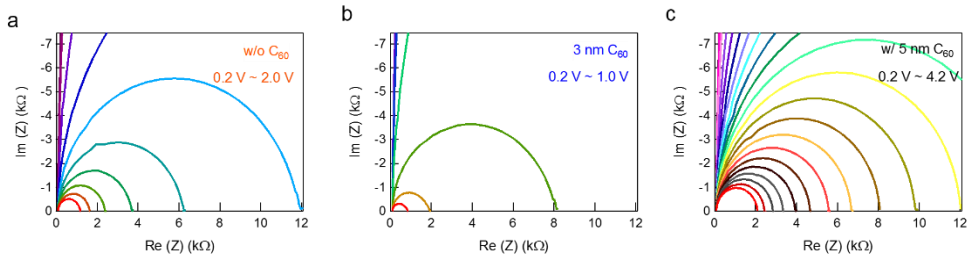

Figure 3.8 Cole-cole plot measured with different voltage (0.2 V ~ 2.0 V), (0.2 V ~ 1.0 V), and (0.2 V ~ 4.2 V) for each HODs with C_{60} thickness of (a) 0, (b) 3, and (c) 5 nm respectively.

Table 3.5. Cole-Cole plot fitting result by Z-View (HOD w/o C_{60} HIIL)

V_{bias} (V)	R_1 (Ω)	R_2 (Ω)	C_1 (nF)	R_3 (Ω)	R_3 Error (%)	C_2 (nF)	C_2 Error (%)
0.2	123.7	2.83E+06	7.56E-01	12983	2.6634	7.85E+00	0.61195
0.4	118.7	6.50E+05	7.62E-01	11085	0.63192	7.07E+00	1.0667
0.6	119.4	66915	8.60E-01	9901	1.5256	3.42E+00	1.3235
0.8	116.8	25161	7.05E-01	2792	1.1213	2.53E+01	0.49072
1.0	116.7	10786	6.98E-01	954.2	0.63364	4.27E+01	0.29433
1.2	120.4	5617	7.01E-01	471.7	0.54958	4.90E+01	0.49222
1.4	140.4	2615	7.31E-01	303.8	0.52431	7.66E+01	0.23454
1.6	155.9	2100	7.51E-01	124.2	0.49857	1.04E+02	1.5259
1.8	174.5	1386	8.09E-01	70.23	0.84271	1.51E+02	2.3317
2.0	199.1	935.1	9.24E-01	38.34	1.3793	2.48E+02	3.4776

Table 3.6 Cole-Cole plot fitting result by Z-View (HOD w/ 3 nm C_{60} HIIL)

V_{bias} (V)	R_1 (Ω)	R_2 (Ω)	C_1 (nF)	R_3 (Ω)	R_3 Error (%)	C_2 (nF)	C_2 Error (%)
0.2	147	3.35E+06	7.70E-01	13640	3.4763	7.59E+00	0.64026
0.3	148.5	7.03E+05	7.90E-01	13514	0.70984	6.20E+00	1.0774
0.4	153.3	99172	7.46E-01	12421	1.1034	9.20E+00	1.0364
0.6	178.3	6978	7.45E-01	919.1	1.2034	3.31E+01	0.78292
0.8	265.6	1450	9.57E-01	203.9	1.7134	7.16E+01	4.8012
1	321.8	471.5	1.95E+00	59.12	3.5383	1.67E+02	9.0726

Table 3.7 Cole-Cole plot fitting result by Z-View (HOD w/ 5 nm C_{60} HIIL)

V_{bias} (V)	R_1 (Ω)	R_2 (Ω)	C_1 (nF)	R_3 (Ω)	R_3 Error (%)	C_2 (nF)	C_2 Error (%)
0.2	113	5.21E+06	7.22E-01	11151	5.6519	7.12E+00	0.59422
0.4	112.3	1.54E+06	7.19E-01	8872	1.5978	7.32E+00	0.64789
0.6	111.9	4.09E+05	7.18E-01	6097	0.50623	7.28E+00	0.94739
0.8	111.1	1.31E+05	7.62E-01	7517	1.7408	4.54E+00	3.263
1	110.6	58042	9.29E-01	12601	7.8727	3.18E+00	1.26
1.6	109.8	12680	9.95E-01	11025	2.181	3.87E+00	1.24
1.8	109.8	11604	8.80E-01	6789	1.7	2.48E+00	12.133
2	109.7	10573	7.92E-01	3982	1.025	3.62E+00	8.3145
2.2	109.6	8964	7.60E-01	2720	8.4453	4.45E+00	6.2486
2.4	108.6	7894	7.17E-01	1598	4.818	6.91E+00	3.3643
2.6	109.2	6909	6.85E-01	867.3	2.3364	1.26E+01	1.4633
2.8	108.6	5785	6.78E-01	629.1	1.9146	1.52E+01	1.1506
3	109.2	4943	6.68E-01	399.8	1.1829	2.41E+01	0.61988
3.2	108.9	4158	6.66E-01	313.6	1.0419	2.74E+01	0.51586
3.4	109.3	3528	6.63E-01	235.4	0.925	3.43E+01	0.41853
3.6	109.1	2998	6.63E-01	193.1	0.71508	3.69E+01	0.30999
3.8	106.1	2525	6.63E-01	186.1	1.0913	3.00E+01	0.4828
4	108.3	2230	6.61E-01	122.1	0.51924	4.99E+01	0.21104
4.2	109.1	1939	6.61E-01	94.41	0.4016	6.43E+01	0.18099

To investigate the origin of enhanced hole transport property of HODs, the electrochemical impedance spectroscopy (EIS) analysis have taken to match with the hole transport property. The EIS was used to study the charge transport and carrier accumulation in a physical and electrical mechanism [79-82]. The impedance was measured over the range of 1 Hz to 0.5 MHz with an oscillation amplitude of 10 mV. Different DC bias range was applied to each devices, 0.2-2.0V for pristine device, 0.2-1.0V, 0.2-4.4V for 3nm, 5nm of C_{60} HIIL respectively. (Figure 3.8)

We extracted resistance and capacitance values by fitting the cole-cole curve using Z-view software. The equivalent circuit to analyze HOD IS data is shown in Figure 3.7c, composed of contact resistance (R_s), transport resistance (R_{tr}), transport capacitance (C_{tr}), interlayer resistance (R_μ) and interlayer capacitance (C_μ). Transport resistance and capacitance stands for hole transport in bulk materials such as CBP and PEDOT:PSS. Interlayer resistance and capacitance, which can be called chemical capacitance, represents the mobile charge carrier density at the interface of CBP and MoO_x. Chemical capacitance extracted by fitting the cole-cole plot of the HOD with different C_{60} HIIL thickness versus DC bias voltage is shown at Figure 3.9. The interlayer capacitance - applied voltage graph matches well with the capacitance-voltage (C-V) curve measure by EIS. (Figure 3.10) 3 nm C_{60} HIIL HODs showed faster the enhancement in C_μ than non-C_{60} HOD and 5 nm C_{60} HIIL HODs showed rather slow enhancement increasing at 3 V. For the accurate comparison with the result of electron-hole injection rate imbalance factor, C_μ value were extracted at 30 mA/cm^2 current density. As the current density enhancement rate in QD-LEDs and HODs showed same, we assumed the interlayer condition of CBP and MoO_x in QD-LEDs and HODs will be similar at the same current density. The interlayer capacitance depending on C_{60} HIIL thickness is shown on Figure 3.9b. We found that the calculated interlayer capacitance versus C_{60} HIIL thickness trend is consistent with

electron-hole imbalance factor trend. This reflects the enhancement in hole injection carrier between HTL and MoO_x reduce QLEDs electron-hole imbalance by enhancing the interlayer property of CBP and MoO_x.

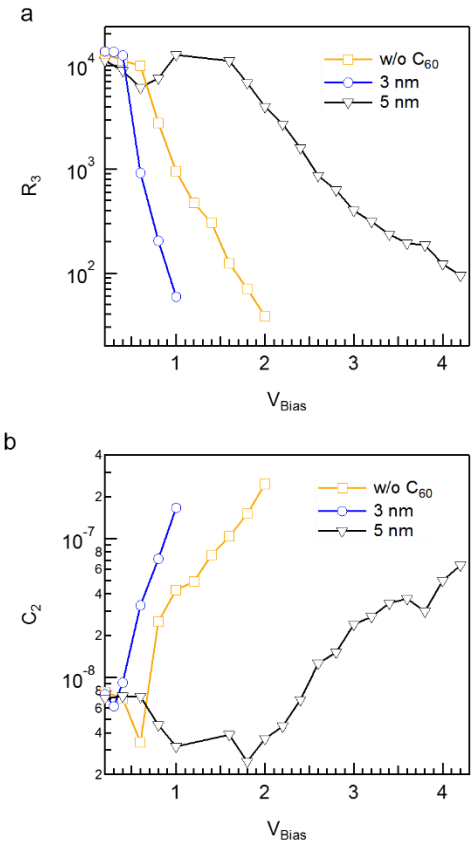

Figure 3.9 Fitting result of HODs with various C_{60} interlayer plotted by applied voltage. (a) Interfacial resistance – applied voltage plot (b) Interfacial capacitance – applied voltage plot.

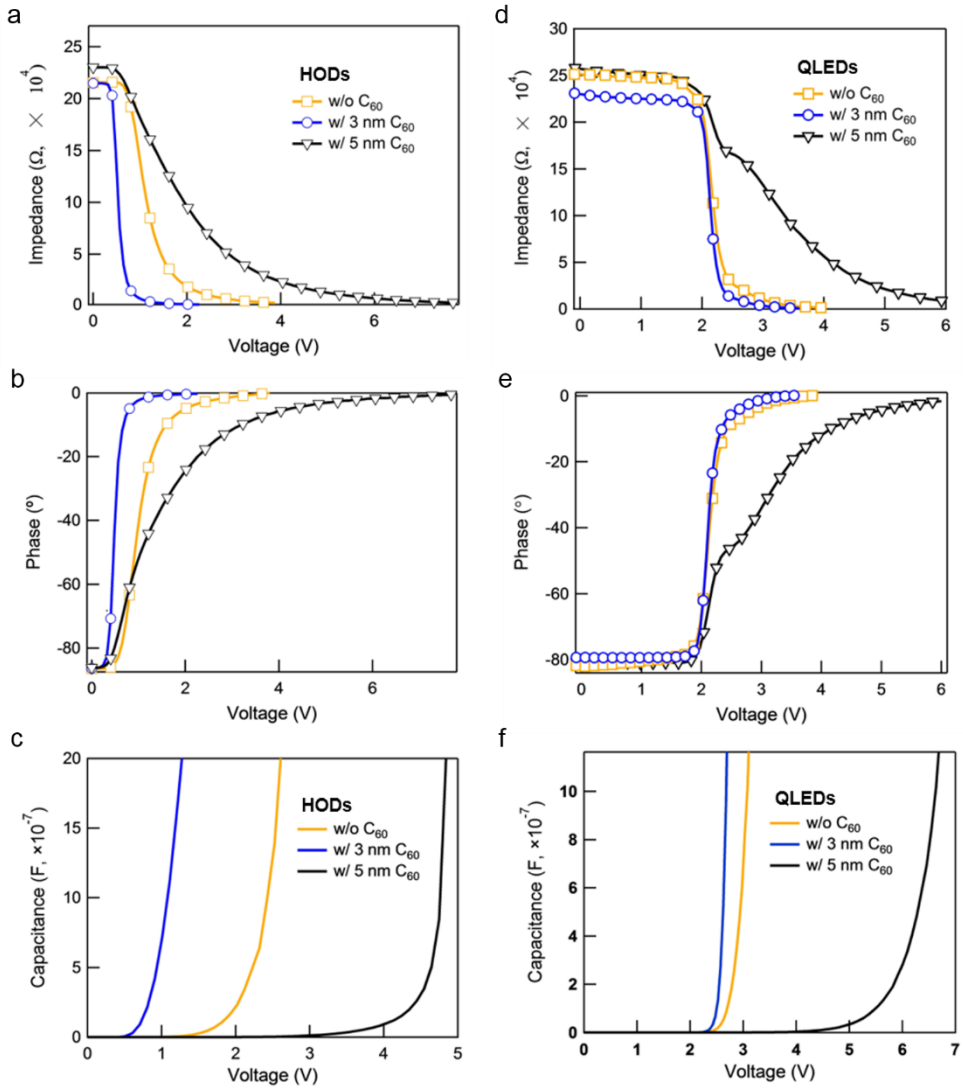

Figure 3.10 Impedance spectroscopy analysis of the HODs and QD-LEDs. (a) Impedance-voltage (b) Phase-voltage (c) Capacitance-voltage characteristics of the HODs and (d) Impedance-voltage (e) Phase-voltage (f) Capacitance-voltage characteristics of the QD-LEDs with the frequency of 1 kHz employing varying thicknesses of C_{60} interlayer.[74]

3.4 Electrical Characteristics of HODs with HIIL analyzed by Temperature Experiment

To confirmed the injection enhancement property of HODs and QD-LEDs by insertion of C_{60} HIIL, the activation energy (E_t) was calculated through temperature dependent J-V measurement (180 ~ 320 K). (Figure 3.11a, b and Figure 3.12a, b) The J-V characteristics show dramatic increase in current at a given voltage with increasing temperature, we surmise this is due to the increase in mobility and decrease in material resistivity of organic hole transport layer with increasing temperature. This is reasonable since mobility in small-molecule organics is essentially a thermally driven process. The J–V characteristics fitted well with the trap charge limited current (TCLC) model, which is reported by Shen et al. [83] The J-V curves of QD-LEDs fitting well with the power law function which can be expressed as [84-86]

$$J = J_0 \exp\left(-\frac{E_A}{k_B T}\right)$$

$$J \propto (V - V_i)^{m+1}$$

Where E_A is activation energy at the largest state density, K_B is Boltzmann constant, V_i is threshold voltage, and m is the slope of log-log plot in the TCLC voltage region. The calculated E_t dependent on the applied voltage is plotted and shown that by inserting thin C_{60} HIIL the activation energy greatly reduced starting at the low voltage region both in HODs and QD-LEDs. In the point of HODs, it is intuitive to estimate the origin of reduced activation energy because the biggest charge transport barrier in the architecture is between CBP and MoO_x. Although the starting activation energy is 80 meV, which is smaller that the 0.3 eV of hole injection barrier

due to the pinning effect of MoO_x, the activation energy abruptly decrease as insertion of thin C_{60} HIIL. On the other hand, the activation energy of pristine HODs barely decreased even at the high applied voltage region. As the previous study shown [75], this can be interpret as insertion of deep HOMO level material can eliminate the universal hole injection barrier.

As a result, we could easily surmise that the insertion of C_{60} reduces hole transport barrier between CBP and MoO_x and resulting alleviation of trap activation energy in the HODs. By considering the result, the reduced activation energy at the QD-LEDs also can be understand that the enhancement of hole injection property results reduction in the activation energy in all applied voltage region. Although the activation energy of pristine QD-LEDs also showed reduced value at high applied voltage, this is surmised as the effect of accumulated electrons in the QDs EML. The accumulated electrons in the QDs EML exude large electronic field which attracts hole carriers from counterpart. However with the insertion of thin C_{60} HIIL, the activation energy of QD-LEDs decreased rapidly with the small applied voltage region.

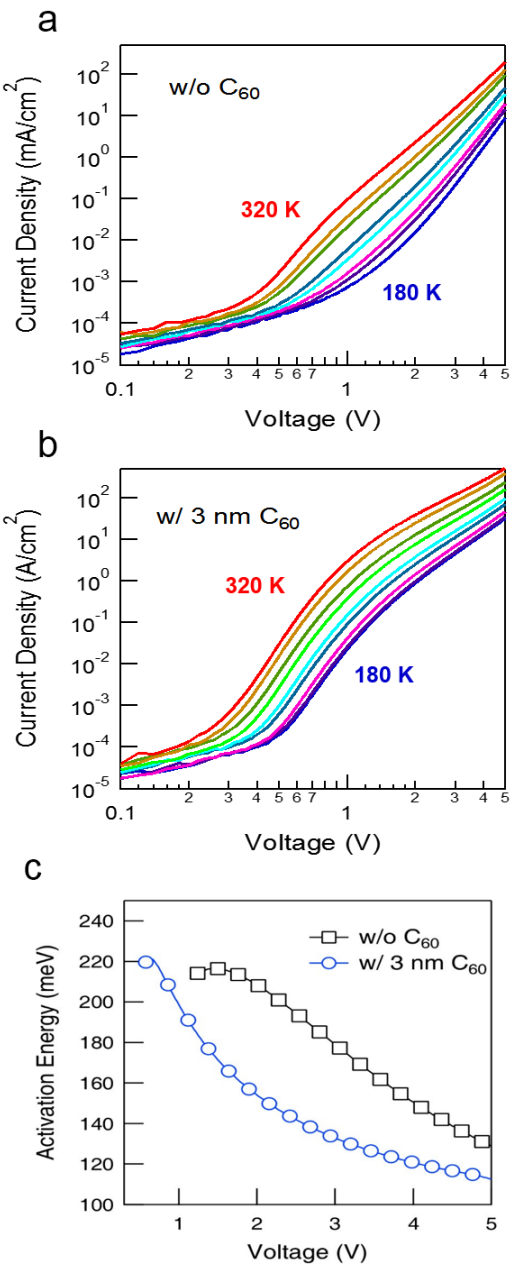

Figure 3.11 Current density – voltage measurement through temperature dependence from 180 K to 320 K of QD-LEDs (a) with C_{60} and (b) without C_{60} HIIL. (c) The calculated activation energy of devices by applying Arrhenius' Equations.

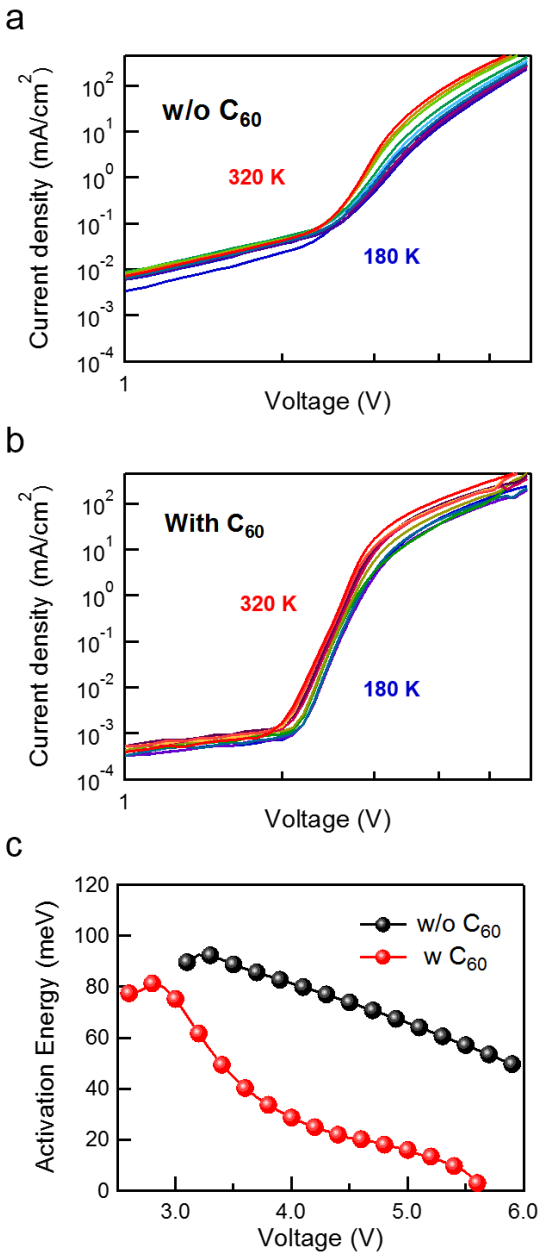

Figure 3.12 Current density – voltage measurement through temperature dependence from 180 K to 320 K of HODs (a) with C_{60} and (b) without C_{60} HIIL. (c) The calculated activation energy of devices by applying Arrhenius' Equations..

The value of m and calculated E_t depend on the temperature was plotted on the Figure 3.13. At all temperature range the devices with thin C_{60} HIIL showed smaller E_t value from 0.02 eV at 320 K and 0.05 eV at 200 K in HODs, and 0.01 eV at 360 k and 0.02 eV at 240 K in QD-LEDs. The E_t increased gradually as the temperature increases.

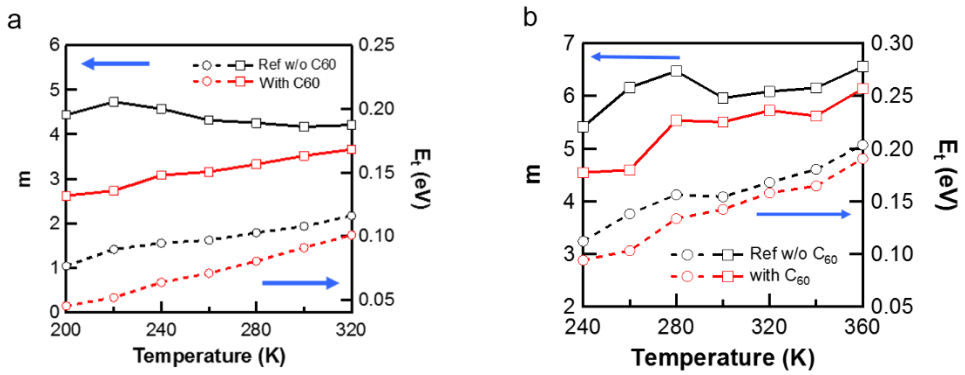

Figure 3.13 Calculated parameter of slope m and activation energy (E_t). Both HODs and (b) QD-LEDs show reduced activation energy factor in all temperature region as insertion of C_{60} interlayer.

3.5 Summary

In summary, we improved the hole injection property of QD-LEDs by inserting a deep HOMO buffer layer (UGH-2, HAT-CN, C60 and BST) between the CBP hole transport layer and the MoO_x hole injection layer. Among them the fullerene (C_{60}) efficiently enhance the hole injection property and resulting overall charge injection balance in the devices. As a result, the QD-LEDs with C_{60} interlayer showed 10% reduced initial rapid luminance drop compared to non- C_{60} interlayer QD-LEDs which leads to 5 times increase in operational lifetime at 1000 nit. (75 % lifetime (LT_{75}) ~ 5.6 hours @ 1000 cd/m^2 for non-C_{60} interlayer QLEDs and (LT_{75}) ~ 36.5 hours @ 1000 cd/m^2 for C_{60} interlayer QD-LEDs).

We systematically analyzed the enhancement of electrical property of devices by impedance spectroscopy and temperature analysis. To remove the hole injection barrier between QDs and CBP (HTL), we fabricate HODs architectures without inserting QDs layer. The impedance spectroscopy analysis result shows that the enhancement of QD-LEDs performance arises from the enhancement hole injection property. By decompose each components in the HODs with the fitting data of applied equivalent circuit, we have conclude that the interface component (Resistance and capacitance) greatly enhanced by the insertion of C_{60} HIIL. By the temperature analysis, this interfacial enhancement property was revalidated.

Chapter 4

Analysis on the Operation Stability of Quantum Dot Light-Emitting Diodes

Despite substantial progress made in the performance, the state-of-the-art QD-LEDs are still in need of operational stability that is a prerequisite factor for their practicable use. The origin of stability degradation of QD-LEDs is unveiled to originate from the charge injection imbalance [45]. The disparity between charge carrier injection rates results in the accumulation of excess charge carriers within the QD emitters that promotes non-radiative Auger recombination processes [46, 47], leading to a reduction of luminance efficiency of QD-LEDs. In addition, the overflow of charge carriers across the QD emissive layer toward counter electrodes provokes degradation of charge transport layers [45, 49, 50] that causes irreversible degradation of QD-LEDs.

Equalized charge carrier injection rates promise a long-lived QD-LED. The most widely attempted approach to reach the charge carrier balance is decelerating the injection rate of dominant charge carriers. Inserting an electron blocking layer at the interface between the electron transport layers (ETL) and the QD emissive layer [4, 52, 54-57, 60] or lowering the carrier mobility of electron transport layers [23, 60, 61] are the representative examples for the state-of-the-art QD-LEDs, in which the injection rate of electrons into QDs far exceeds that of hole. These negative incentives permit the increase in the device efficiency, but simultaneously accompany an unwanted outcome, the increase in the operation voltage to gain the fixed current density, that could accelerate degradation of the device by Joule heating.

In the previous chapter, we presented a "positive incentive" approach to enhance the operational stability of QD-LEDs by inserting a thin fullerene (C_{60}) interlayer. The insertion of thin layer changed electrical and optical property of QD-LEDs and HODs. In this chapter by applying the unique structural feature, we quantitatively assess the extent of charge injection imbalance within the QD emissive layer from combined analysis on electrical properties of QD-LEDs and photophysical properties of the QD emissive layer within the devices, and discuss their impact to optoelectronic performance and operational stability of QD-LEDs.

4.1 Lifetime Characteristics of Electroluminescence Devices assisted by Deep HOMO Level HIIL

In the previous chapter, we presented an enhanced performance and lifetime of QD-LEDs by inserting a thin fullerene (C_{60}) HIIL. Compared to conventional architecture of QD-LEDs, the proposed structure only differs by the insertion of thin (~ 5 nm) C_{60} HIIL between CBP (HTL) and MoO_x (HIL). (Figure 4.1) However the electroluminescence property enhanced greatly due to the increase of minority carrier (Hole carrier) of the QD-LEDs. Compared in the same operated current density, the QD-LEDs with C_{60} interlayer applied low operational voltage compared to that of QD-LEDs without C_{60} interlayer. This characteristic is excellent system for comparing the operational stability of two different QD-LEDs which has nearly same device architecture due to the minimization of variation of experiment.

We briefly discussed the lifetime characteristics of QD-LEDs with varying C_{60} HIIL in the previous chapter. The QD-LEDs with 3 nm C_{60} interlayer showed 10% reduced initial rapid luminance drop compared to non- C_{60} interlayer QD-LEDs which leads to 5 times increase in operational lifetime at 1000 nit. (75 % lifetime (LT_{75}) ~ 5.6 hours @ 1000 cd/m^2 for non-C_{60} interlayer QLEDs and (LT_{75}) ~ 36.5 hours @ 1000 cd/m^2 for 3 nm C_{60} interlayer QD-LEDs). However, the operational condition such as operational current density and operational voltage is largely different with the thickness of C_{60} HIIL. The operational current density at 1000 cd/m^2 is 22.83, 19.15, and 24.13 mA/cm^2 for QD-LEDs with 0, 3, and 5 nm C_{60} HIIL respectively. The initial operational voltage at 1000 cd/m^2 is 4.1, 3.5, and 6.4 mA/cm2 for QD-LEDs with0, 3, and 5 nm C_{60} HIIL respectively. (Figure 4.2 and Table 4.1) Although QD-LEDs with 3 nm C_{60} HIIL shows most prolonged lifetime, the origin of operational stability is veiled. When we compare lifetime in same luminance

condition for all devices, the operational conditions (Operational current density, applied voltage, and charge imbalance factor) will be different in all devices and undesirable for finding the impact of key factors that deteriorate QD-LEDs. Therefore to investigate the operational stability of QD-LEDs, it is prerequisite to compare them not in the same luminance conditions, but in the same operational conditions, such as current density or applied voltage. Comparative analysis among QD-LEDs with varying interlayer thicknesses both at the low current regime (J = 30 mA/cm^2, L = 1,000-2000 cd/m^2) and the high current density regime (J = 200 mA/cm^2, L = 10,000 cd/m^2) will enable us to understand the impact of the device characteristics (e.g., charge injection imbalance, operation voltage) on the operational stability of QD-LEDs

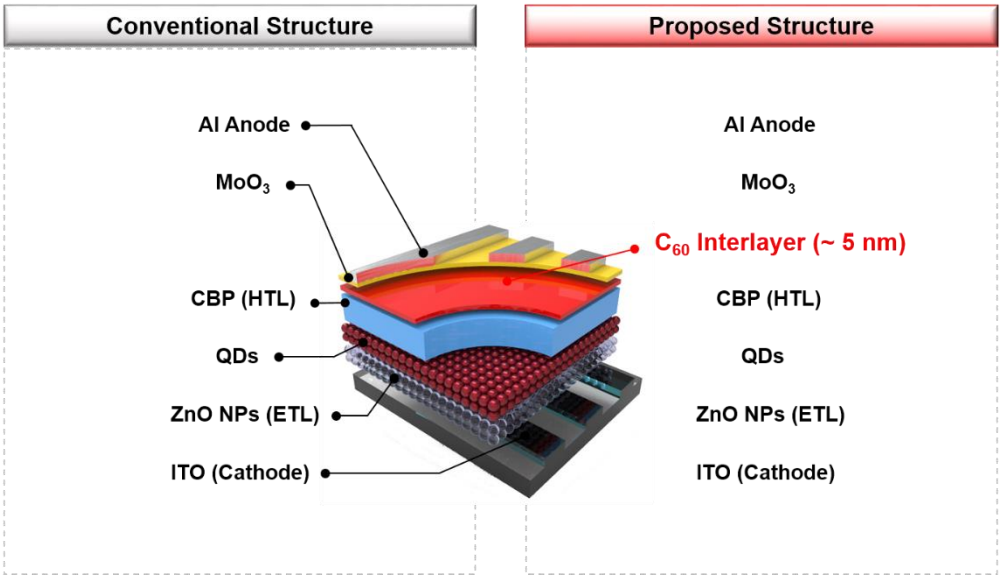

Figure 4.1 Structural uniqueness for analyzing the operational stability of QD-LEDs. The proposed structure only differs in the thin (~ 5 nm) C_{60} HIIL.

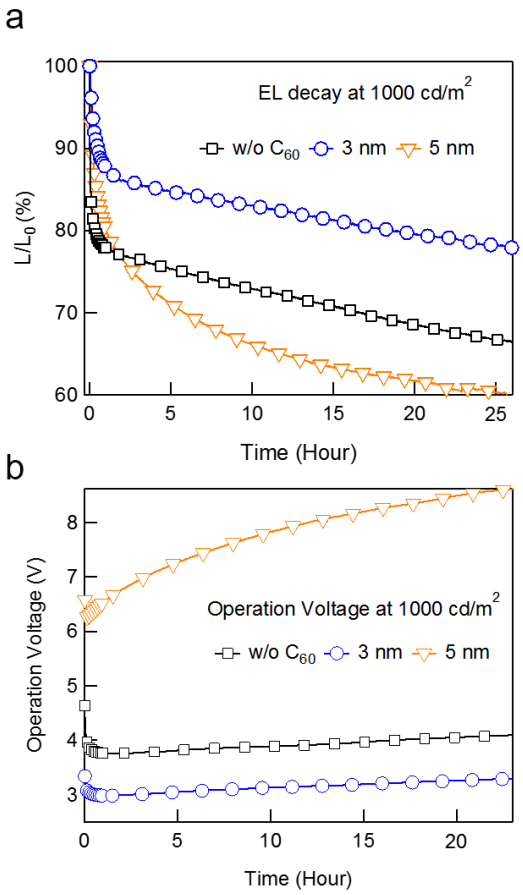

Figure 4.2 Lifetime characteristics of QD-LEDs by controlling the thickness of C_{60} HIIL. Time dependent (a) luminance decay graph and (b) operated voltage graph. Initial luminance (L_0) is 1000 cd/m^2.

Table 4.1 Operational current density for 1000 cd/m^2 of QD-LEDs with varying thickness of C_{60} HIIL

	w/o C_{60}	**3 nm**	**5 nm**
Operation Current Density @ 1000 cd/m^2 [mA/cm^2]	22.83	19.15	24.13

4.2 Characteristics of Electroluminescence and Photoluminescence of QD based LED assisted by Deep HOMO Level HIIL

We assess the operation stability of QD-LEDs by monitoring the electroluminescence (EL) traces as a function of the operation time at the constant current density (Figure 4.3). Concurrently, we also monitor the traces of photophysical characteristics of the QD emissive layers within the working devices and estimate the degree of QD charging and its contribution to the efficiency drop of devices. Irrespective of the operation current density, the device efficiency of QD-LEDs declines in two steps:[45] the rapid decrease in the device efficiency at the early operation stage accompanying PL QY loss of the QD emissive layer (Stage I) and the slow but steady decay of the device efficiency after the PL QY of the QD emissive layer ceases to decrease (Stage II). (Figure 4.5a) We estimate the degree of charge injection imbalance into the QD active layers ($(J_{e0}-J_h)/J_{e0}$) from the PL QY decay dynamics and correlate it with the device efficiency and the operational stability. We define the switch time from Stage I to Stage II (T_1) when ca. 98 % of PL QY decay completes and rescale the device efficiency curves from T1 to evaluate the device decay rate at Stage II.

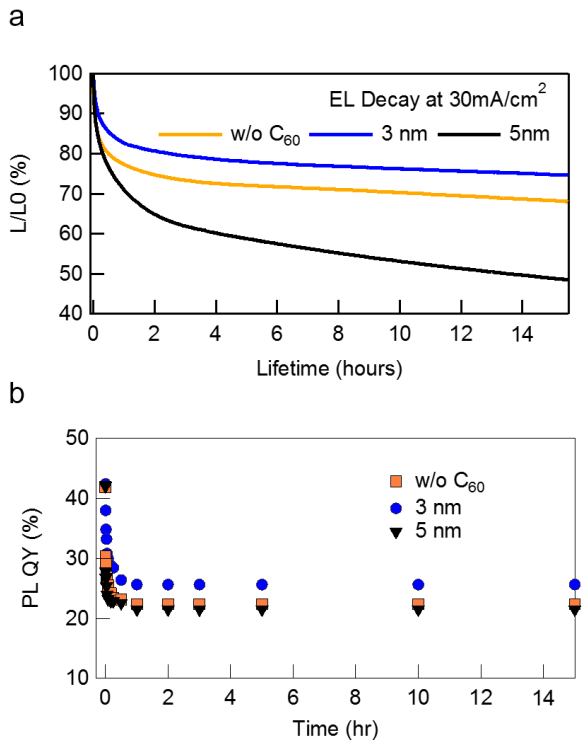

Figure 4.3 Changes in optical characteristics of the QD emissive layer under the device operation (a) luminance decay trend of QD-LEDs with varying C_{60} interlayer thickness (0, 3, 5 nm) which could eventually correspond to internal quantum efficiency (IQE) trend (b) PL QY decay trend of QD which is operated under the constant current density.

Charge injection imbalance ($(J_{e0}-J_h)/J_{e0}$) is calculated by using QD charging model [45]. The fraction of negatively charged QDs and the electron injection rate at a given time ($\boldsymbol{J(t)}$) under constant current density ($\boldsymbol{J_h}$ = constant) can be obtained by considering coupled rate equations. (Figure 4.4)

$$J_e(t) - J_h = \frac{dC(t)}{dt}$$

$$J_e(t) = J_e(0)(1 - \alpha \frac{C(t)}{N})$$

where $J_e(t)$ and J_h is the number of injected electrons and holes into QDs in unit area (cm^2) at time t, N is the number of QDs in unit area (cm^2), C(t) is the number of charged QDs in unit area (cm^2) at time t, and α is the repulsion coefficient for electron injection from ZnO ETL into negatively charged QDs.

From these equations, we can get the fraction of charged QDs and the electron injection rate at a given time ($J_e(t)$).

$$F(t) = \frac{C(t)}{N} = \frac{J_e(0) - J_h}{J_e(0)}(1 - \exp\left(-\frac{J_e(0)\alpha}{N}t\right))$$

$$J_e(t) = J_e(0) - (J_e(0) - J_h)(1 - \exp\left(-\frac{J_e(0)\alpha}{N}t\right))$$

When QD is fully charged, remaining efficiency and the fraction of charged QD (F) correlate with injection imbalance.

$$F = 1 - \frac{B}{A} \propto \frac{J_e(0) - J_h}{J_e(0)}$$

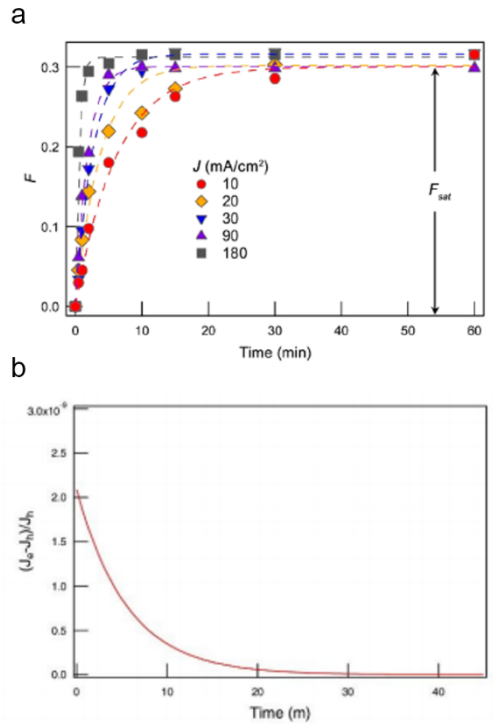

Figure 4.4 Influence of the structural formulations of QDs on the early efficiency drop in QLEDs. Operation time-dependent traces of the fraction of charged QDs (F) in the QD emissive layer of (a) QLEDs implementing CdSe (r = 2.0 nm)/$Zn_{0.5}Cd_{0.5}S$(h = 6.3 nm) type I QDs under the current densities of 10, 20, 30, 90, and 180 mA/cm^2. (b) The imbalance between electron and hole injection rate ($(J_e-J_h)/J_h$) as a function of operation time. (This work is from the reference [45])

The fitting data of IQE and PL QY is illustrated at Figure 4.5. The operation stability of QD-LEDs with varying C_{60} interlayer thicknesses under operation at 30 mA/cm^2. The degradation trend of QD-LEDs at Stage I matches well with the decay trend observed in PL QY of the QD emissive layer, indicating that the rapid decrease in the device efficiency at Stage I is predominantly attributed to the luminescence efficiency loss of the QD emissive film via QD charging and subsequent non-radiative

Auger recombination processes. The similarity enables us to extract the initial charge injection imbalance into QDs in working devices (t = 0) from PL QY traces. Figure 4.5b compares the device efficiency and the charge injection imbalance of QD-LEDs employing varying thicknesses of C_{60} interlayer at the initial operation time (t = 0). The initial device efficiency (EQE (0)) is inversely proportional to the initial charge injection imbalance ($(J_{e0}-J_h)/J_{e0}$) in chosen variation of C_{60} interlayer thickness, implying that the device efficiency enhancement by the presence of C_{60} interlayer is an outcome of the mitigated charge injection imbalance into the QD emissive layer. The reduction of the charge injection imbalance by implanting C_{60} interlayers aids to suppress the extent of the device efficiency drop by QD charging at Stage I and also delays the device degradation at Stage I.

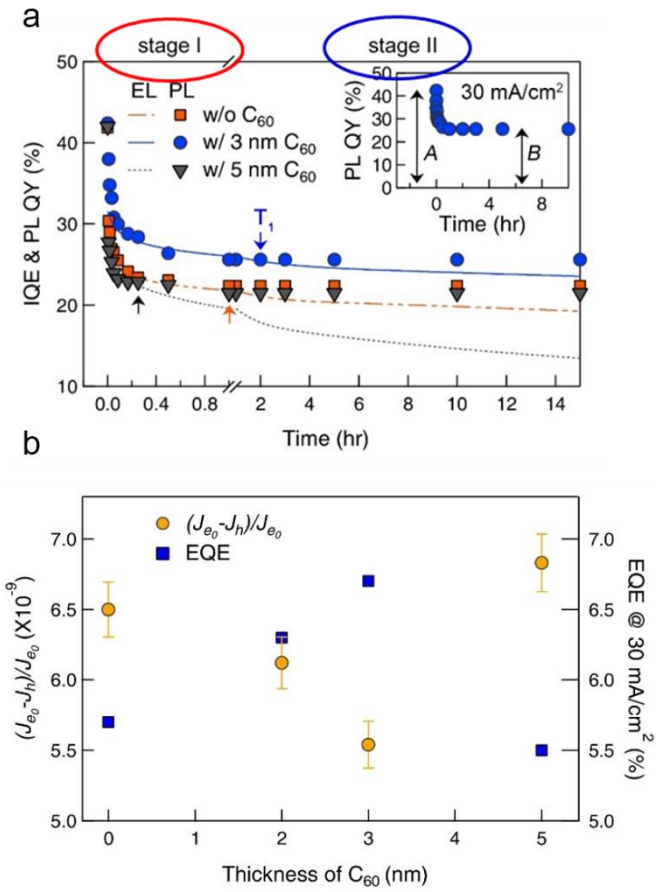

Figure 4.5 (a) Operation time dependent-traces of internal quantum efficiencies (IQEs) of QD-LEDs employing varying thicknesses of C_{60} interlayer. Photoluminescence quantum yields (PL QYs) of QD emissive layers within corresponding devices are overlaid for comparison. An inset shows the change in PL QY of the QD emissive layer under operation at 30 mA/cm^2. (b) The degree of the initial charge injection imbalance ($(J_{e0}-J_h)/J_{e0}$) in QD-LEDs and EQEs at 30 mA/cm^2 depending on the C_{60} interlayer thickness. All QD-LEDs were operated at a constant current density of 30 mA/cm^2.[74]

The device degradation rates at Stage I (K_I) and the extent of efficiency drops at Stage I are linearly correlate with the initial charge injection imbalance ($(J_{e0}-J_h)/J_{e0}$). These results validate the previous model that rationalizes QD-LED degradation at Stage I with the luminescence efficiency loss of the QD emissive layers via QD charging and subsequent non-radiative Auger recombination processes. The insertion of C_{60} interlayers also aids to impede the device degradation rate at Stage II (Figure 4.6). As depicted in Figure 4.5b, the charge imbalance factors are deeply related with the EQE of device. As a result, comparing operational stability of QD-LEDs only in the same applied current density is insufficient, resulting the prolonged devices determined by the EQE value of the devices. Therefore for all-else-being-equal conditions, it is necessary to conduct analysis of operational stability not only at the same operational current density but also at the point where all devices has same EQE. We choose 200 mA/cm^2 as the point where the devices shows nearly similar EQE, and conducted 3 different applied current density points of analysis on the operational stability of QD-LEDs with various C_{60} interlayer thickness (0, 3, and 5 nm). The electroluminescence characteristics of QD-LEDs with 0, 3, and 5 nm C_{60} interlayer is shown in the Table 4.2.

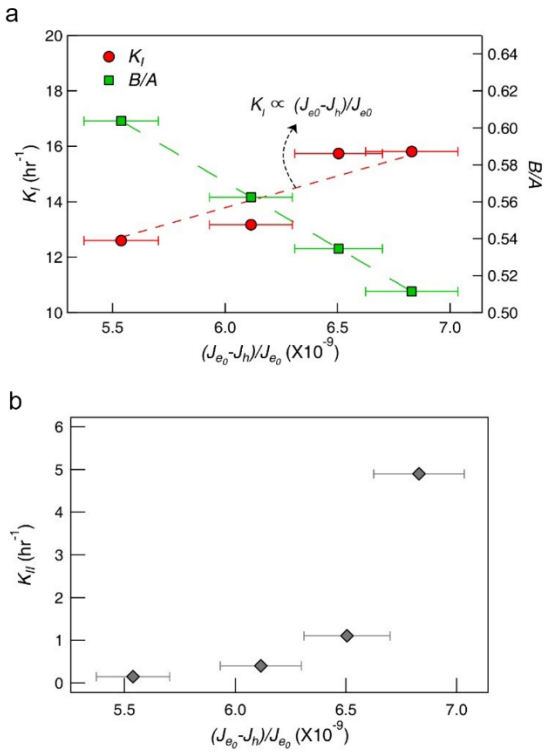

Figure 4.6 (a) Device degradation rates at Stage I (K_I) and the ratio between the initial PL QY and the remaining PL QY of the QD emissive layer (B/A). (b) Device degradation rates at Stage II (K_{II}) as a function of the degree of initial electron-hole injection imbalance into QDs ($(J_{e0}-J_h)/J_{e0}$). All QD-LEDs were operated at a constant current density of 30 mA/cm^2.[74]

Table 4.2 Electroluminescence characteristics of QD-LEDs with varying thicknesses of C_{60} interlayer at current densities of 30, 100 and 200 mA/cm^2.

30 mA/cm^2	EQE (%)	Voltage (V)	Luminance (NIT)
w/o C_{60}	5.7	4.1	1,320
3 nm C_{60}	6.7	3.7	1,570
5 nm C_{60}	5.5	6.4	1,280

100 mA/cm^2	EQE (%)	Voltage (V)	Luminance (NIT)
w/o C_{60}	6.1	4.6	4,700
3 nm C_{60}	6.5	3.9	5,000
5 nm C_{60}	5.8	7.1	4,400

200 mA/cm^2	EQE (%)	Voltage (V)	Luminance (NIT)
w/o C_{60}	**6.3**	5.1	10,600
3 nm C_{60}	**6.4**	4.2	10,700
5 nm C_{60}	5.5	7.6	9,200

4.3 Quantitative Assessment of Operational Stability of Electroluminescence Devices

For all-else-being-equal conditions, it is necessary to conduct analysis of operational stability not only at the same operational current density but also at the point where all devices has same EQE. We choose 200 mA/cm^2 as the point where the devices shows nearly similar EQE (6.3 % and 6.4 % for pristine QD-LEDs and 3 nm C_{60} interlayer QD-LEDs respectively), and conducted 3 different applied current density points (30, 100, and 200 mA/cm^2) of analysis on the operational stability of QD-LEDs with various C_{60} interlayer thickness (0, 3, and 5 nm). The comparative analysis among QD-LEDs with varying interlayer thicknesses both at the low current regime (J = 30 mA/cm^2, L = 1,000-2000 cd/m^2) and the high current density regime (J = 200 mA/cm^2, L = 10,000 cd/m^2) enables us to understand the impact of the device characteristics (e.g., charge injection imbalance, operation voltage) on the operational stability of QD-LEDs

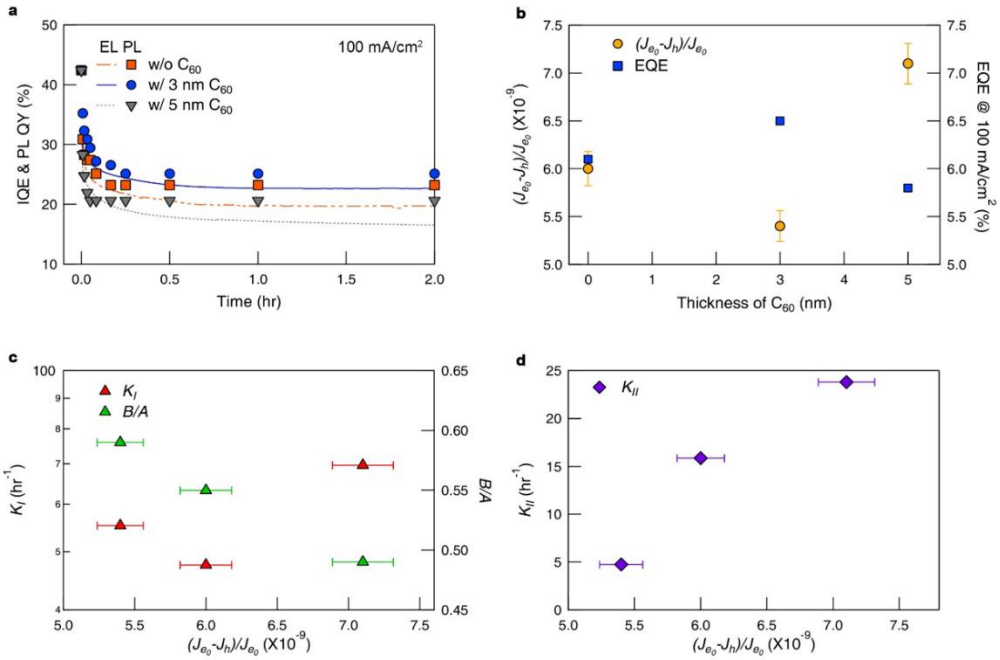

Figure 4.7 Degradation trends of QD-LEDs with varying thicknesses of C_{60} interlayer at high current density (100 mA/cm^2). (a) Operation time dependent PL QY of QD emissive layer within device and IQE of QD-LEDs with varying thicknesses of C_{60} interlayer. (b) The degree of the initial charge injection imbalance ($(J_{e0}-J_h)/J_{e0}$) in QD-LEDs and EQEs at 100 mA/cm^2 depending on the C_{60} interlayer thickness. (c) Device degradation rates of Stage I (K_I), remaining efficiency (B/A) and (d) device degradation rates at Stage II (K_{II}) as a function of the degree of initial electron-hole injection imbalance into QDs ($(J_{e0}-J_h)/J_{e0}$). All QD-LEDs were operated at a constant current density of 100 mA/cm^2.[74]

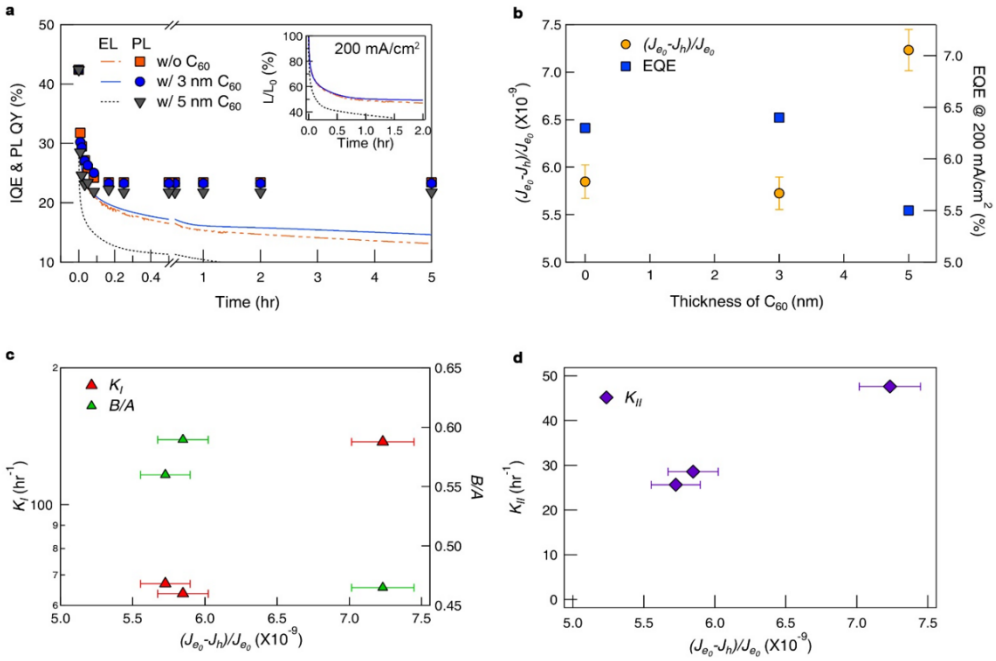

Figure 4.8 Degradation trends of QD-LEDs with varying thicknesses of C_{60} interlayer at high current density (200 mA/cm^2). (a) Operation time dependent PL QY of QD emissive layer within device and IQE of QD-LEDs with varying thicknesses of C_{60} interlayer. (b) The degree of the initial charge injection imbalance ($(J_{e0}-J_h)/J_{e0}$) in QD-LEDs and EQEs at 200 mA/cm^2 depending on the C_{60} interlayer thickness. (c) Device degradation rates of Stage I (K_I), remaining efficiency (B/A) and (d) device degradation rates at Stage II (K_{II}) as a function of the degree of initial electron-hole injection imbalance into QDs ($(J_{e0}-J_h)/J_{e0}$). All QD-LEDs were operated at a constant current density of 200 mA/cm^2.[74]

4.4 Characteristics of Operational Stability of QD based LED based on All-Else-Being-Equal Conditions

We conduct the device operational stability tests under operation at 100 mA/cm^2 and 200 mA/cm^2, where the device efficiency barley changes upon the variation in C_{60} interlayer thickness (Figure 4.7 and 4.8) and summarize the relationships between the device operation stability and the device characteristics (Figure 4.9 and 4.10). The device degradation rates at both Stage I (K_I) and Stage II (K_{II}) have linear relationships with the charge carrier injection imbalance into QDs (J_{e0}-J_h) (Figure 4.10). The extent of efficiency drop at Stage I (1-B/A) is linearly proportional to the extent of the initial charge injection imbalance ((J_{e0}-J_h)/J_{e0}) (Figure 4.9). These results consistently attest that the disparity of charge carrier injection rate is the primary reason for the device degradation at both Stage I and Stage II. The charge injection imbalance yields the accumulation of excess charge carriers within the QD emissive layer that escalates the probability of non-radiative Auger recombination processes, leading to the device efficiency drop at Stage I. The leakage of extra charge carriers accumulated in the QD emissive layer toward counter CTLs causes structural deformation of CTLs (here, CBP) that becomes charge carrier traps and reduces the device efficiency at Stage II.

Both the device degradation rate and the extent of device efficiency at Stage I disregard the influence of the applied voltage. By contrast, the device degradation rate at Stage II is primarily determined by the charge injection imbalance and also influenced by the applied voltage (Figure 4.10b). We attribute the reason to the origin of device degradation at stage II that involves irreversible degradation of HTL via chemical reaction. In the present case, exocyclic C-N bond in CBP is known as a weak bond and liable to undergo structural deformation that creates deep trap sites. The electrons that escape from the QD emissive layer toward HTL play a decisive role in

the HTL degradation processes, and higher applied voltage and subsequent heat supply to the system expedite the electron leakage to HTLs and consequently the HTL degradation. The insertion of 3 nm thick C60 interlayer not only enhances the charge injection balance within the QD emissive layer but also reduces the operation voltage by ~ 0.4 V, 0.7 V and 0.9 V for operating 30, 100 and 200 mA/cm^2. As a combined result of suppressed charge leakage and the lowered Joule heating, QD-LED employing 3 nm thick C_{60} interlayer displays enhancement in the device stability at Stage II compared to the reference ones (without C_{60} interlayer) under varying operation current densities (Figure 4.10b). We note that the device operation instability of QD-LEDs is strongly related with the charge injection imbalance and the operation voltage rather than the single exciton luminescence efficiency (PL QD) of QDs or the extraction efficiency (η_{out}).

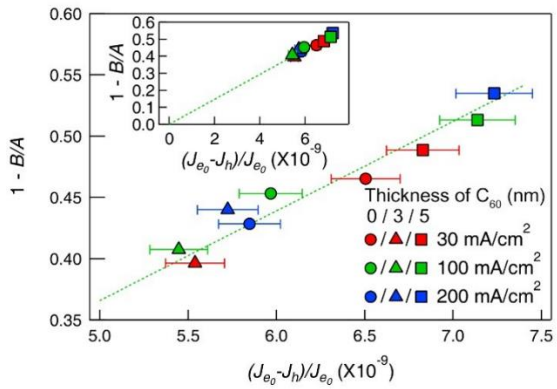

Figure 4.9 QD-LED degradation characteristics: Efficiency loss of the QD emissive layer by QD charging (1-B/A) versus the extent of the initial charge injection imbalance ($(J_{e0}-J_h)/J_{e0}$). The inset extrapolates the efficiency loss by QD charging in QD-LEDs at the equalized charge injection condition ($(J_{e0}-J_h)/J_{e0}=0$).[74]

The decay rates estimated from the fitted lines approximate to nearly 0 for the case with complete charge injection balance ((J_{e0}-J_h) = 0), promising the complete suppression of device degradation under operation. The present approach, eliminating the hole blocking barrier at the interface between cathode and HTL with insertion of C_{60} interlayer, is an effective way of improving the hole current from cathode to HTL, but the outcome that we could achieve in working devices appears to be rather limited. Specifically, HOD experiments imply that the optimum thickness C_{60} interlayer can boost the hole current from cathode into HTL by approximately one order of magnitude, but the enhancement of charge injection imbalance in the QD emissive layer within working devices appears to be at most 10 %. The notable gap between enhancements of the hole current versus charge injection balance is attributed to the energy barrier for hole injection at the interface between HTL and QDs. This in return suggests that, in addition to the present approach, the reduction of hole injection barrier between the QD emissive layer and HTL is necessary to accomplish the complete charge balance in the QD emissive layer. We consider that engineering at the interface between QDs and HTL, for example, reducing the ligand length [87] or lowering the energy barrier of the shell [34, 88, 89], will further boost the hole injection into QDs and eventually enable the complete charge injection balance.

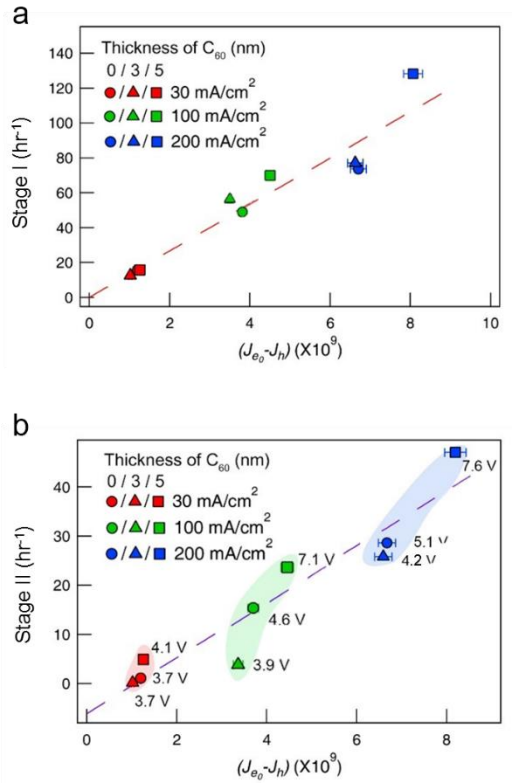

Figure 4.10 QD-LED degradation characteristics: (a) The degradation rate at Stage I (K_I) versus the initial charge injection imbalance into QDs (J_{e0}-J_h). (b) device degradation rates at Stage II (K_{II}) versus the initial charge injection imbalance into QDs (J_{e0}-J_h).[74]

Table 4.3 Electroluminescence characteristics of QD-LEDs with varying thicknesses of C_{60} interlayer at current densities of 30, 100 and 200 mA/cm^2.[74]

	EQE* (%)	Voltage* (V)	Luminance* (NIT)	K_I (hr^{-1})	K_{II} (hr^{-1})	$(Je_0-J_h)/Je_0$ ($\times10^{-9}$)	B/A
30 mA/cm^2							
w/o C_{60}	5.7	4.1	1,320	15.7	1.1	6.5	0.53
2 nm C_{60}	6.3	3.7	1,410	13.2	0.4	6.1	0.56
3 nm C_{60}	6.7	3.7	1,570	12.6	0.2	5.5	0.60
5 nm C_{60}	5.5	6.4	1,280	15.8	4.9	6.8	0.51
100 mA/cm^2							
w/o C_{60}	6.1	4.6	4,700	47.5	15.9	6.0	0.55
3 nm C_{60}	6.5	3.9	5,000	55.3	4.8	5.4	0.59
5 nm C_{60}	5.8	7.1	4,400	69.6	23.8	7.1	0.49
200 mA/cm^2							
w/o C_{60}	6.3	5.1	10,600	63.7	28.6	5.8	0.59
3 nm C_{60}	6.4	4.2	10,700	67.0	25.6	5.7	0.56
5 nm C_{60}	5.5	7.6	9,200	137.4	47.6	7.2	0.46

* Device characteristics at the initial operation (t=0).

4.5 Characteristics of Operational Stability of QD based LED with various HTL

In the previous section, we identified the relation between operational conditions and lifetime of QD-LEDs. However, although we conducted the measurement of operational stability of QD-LEDs which is shows general tendency in QD-LEDs, there should be a verification with the different QD-LEDs structure. Therefore we conducted same stability analysis with the 26DCzPPy (2,6-bis[3-(9H-Carbazol-9-yl)phenyl]pyridine) HTL, which has -6.05 eV of HOMO level and -2.65 eV of LUMO level with relatively high T_g (102 ˚C).

The EL characteristics of 26DCzPPy based QD-LEDs with and without C_{60} interlayer is shown in figure 4.11. The enhancement trend showed consistent trend with the previous CBP based QD-LEDs results. Reduced turn-on voltage and increased EQE at low current density region. Also the operational stability comparison with the constant current density of 30 mA/cm^2 and 100 mA/cm^2. The stability of 26DCzPPy based QD-LEDs with C_{60} interlayer showed prolonged lifetime compared to that of pristine QD-LEDs.

The degradation characteristics of 26DCzPPy based QD–LEDs is shown in figure 3.12. The decay rates estimated from the fitted lines approximate to nearly 0 for the case with complete charge injection balance ((J_{e0}-J_h) = 0), which is consistent with the CBP based QD-LEDs result. Also the Stage II linearly followed the charge injection imbalance and marginally follows the operational voltages at each current density points. This result showed that our stability analysis systems can be applied to various HTL based QD-LEDs.

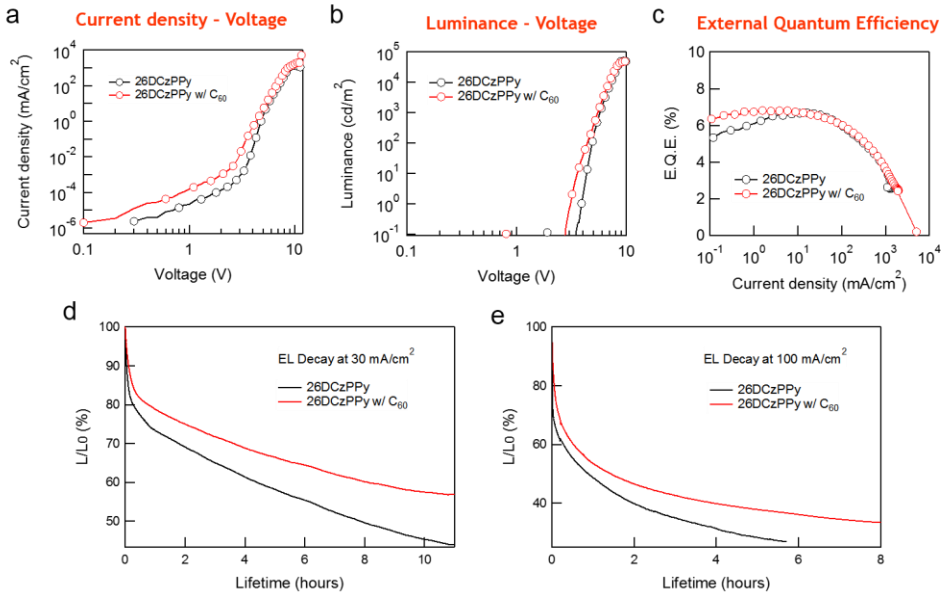

Figure 4.11 EL characteristics (a) Current density-voltage (b) voltage-luminance curves and (c) current density dependent device efficiencies (EQE). Luminance decay trend of QD-LEDs with and without C_{60} interlayer (3 nm) which is operated under the constant current density (d) 30 mA/cm^2 and (e) 100 mA/cm^2.

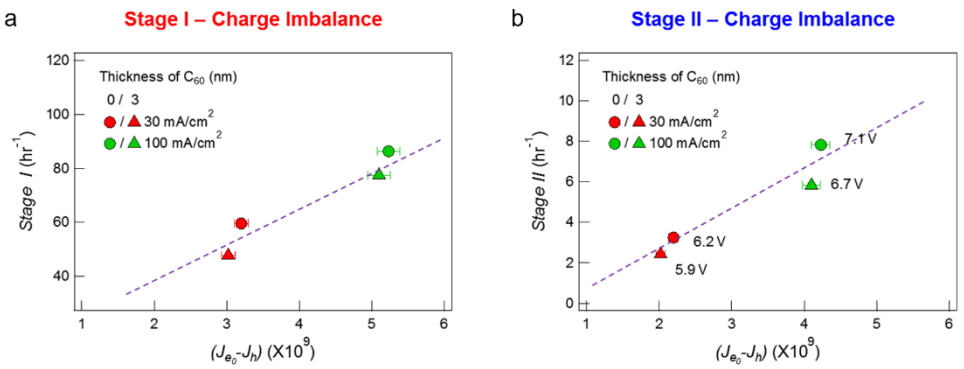

Figure 4.12 26DCzPPy based QD-LED degradation characteristics: (a) The degradation rate at Stage I (K_I) and (b) Stage II (K_{II}) versus the initial charge injection imbalance into QDs (J_{e0}-J_h).

4.6 Effect of Joule Heating on the Electroluminescence Devices

We have identified the operational voltage mainly effect the long term of operational stability in QD-LEDs (Stage II). We attribute the reason to the origin of device degradation at stage II that involves irreversible degradation of HTL via chemical reaction. In the present case, exocyclic C-N bond in CBP is known as a weak bond and liable to undergo structural deformation that creates deep trap sites. The electrons that escape from the QD emissive layer toward HTL play a decisive role in the HTL degradation processes, and higher applied voltage and subsequent heat supply to the system expedite the electron leakage to HTLs and consequently the HTL degradation.

It is well known that CBP has low thermal stability. (T_g = 62˚C) There has been a lot of studies to enhance the thermal stability of CBP by changing the chemical architecture, especially the exchanging the hydrogen on the carbazole side by C-N bond. Thus, the Joule heat generation during device operation may have critical effect on the QD-LEDs. To identify the temperature of devices which rises from Joule heating, we measured the temperature of QD-LEDs on the operation conditions (From 30 mA/cm^2 to 250 mA/cm^2) by IR-camera. (Figure 4.11) The temperature trend followed as the increased applied current density. The maximum temperature of each pixel was 33.1, 30.9, and 43.1˚C for QD-LEDs with 0, 3, and 5 nm C_{60} interlayer. From the Figure 4.12, the temperature strongly influenced by the current density and applied voltage, which eventually gives us to importance of low operational condition on the device operational stability.

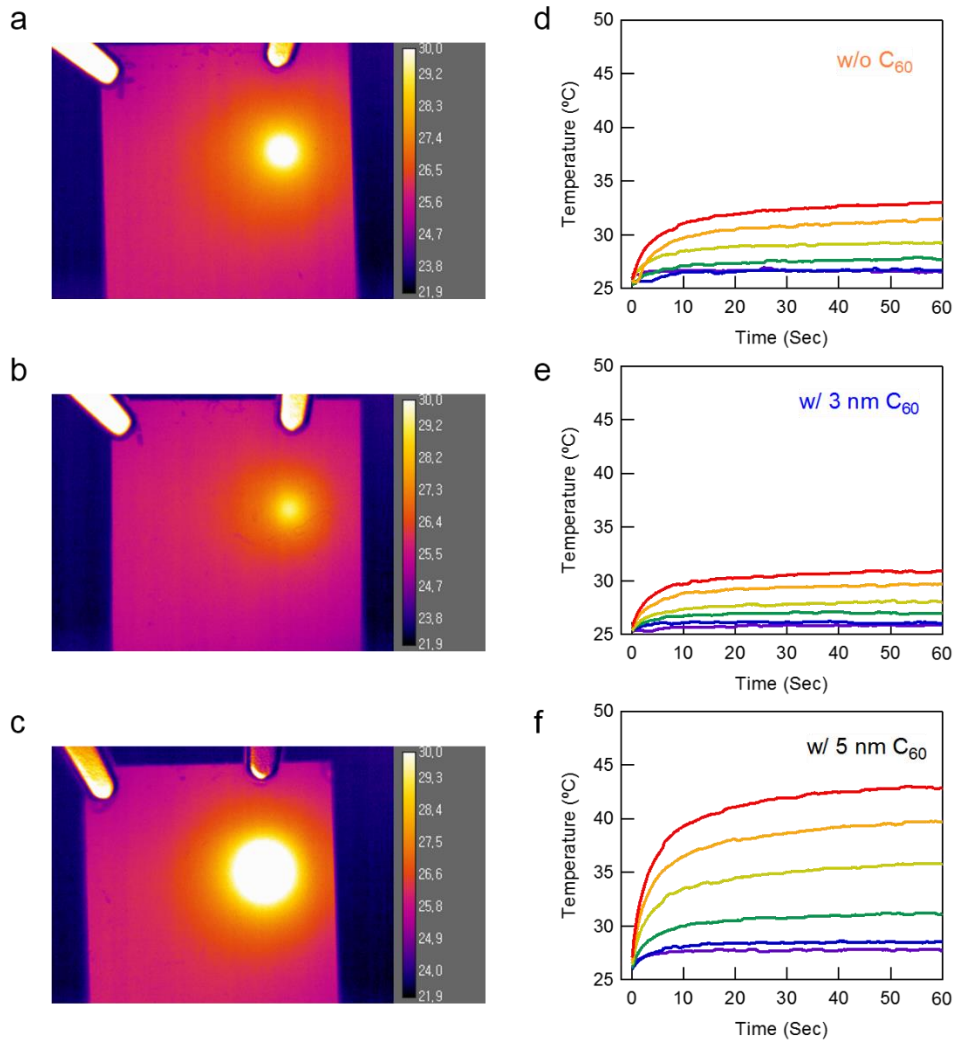

Figure 4.13 Pixel temperature on the operation conditions. (a~c) Pictures taken by IR-Camera of QD-LEDs with 0, 3, and 5 nm C_{60} interlayer (Applied current density from 30 to 250 mA/cm^2). (d~f) Temperature variation depend on the operational time.

Table 4.4 Temperature characteristics of operated QD-LEDs with 0, 3, and 5 nm of C_{60} interlayer (Applied current density from 30 to 250 mA/cm^2).

w/o C_{60}	30 mA/cm^2	50 mA/cm^2	100 mA/cm^2	150 mA/cm^2	200 mA/cm^2	250 mA/cm^2
Voltage (V)	4.0	4.2	4.6	4.8	5.0	5.2
J*V	120	210	460	720	1000	1300
Temperature (°C)	26.6	26.7	27.8	29.3	31.5	33.1
3 nm C_{60}	30 mA/cm^2	50 mA/cm^2	100 mA/cm^2	150 mA/cm^2	200 mA/cm^2	250 mA/cm^2
Voltage (V)	3.7	3.8	4.0	4.2	4.3	4.4
J*V	111	190	400	630	860	1100
Temperature (°C)	25.9	26.0	27.0	28.1	29.8	30.9
5 nm C_{60}	30 mA/cm^2	50 mA/cm^2	100 mA/cm^2	150 mA/cm^2	200 mA/cm^2	250 mA/cm^2
Voltage (V)	5.1	5.8	7.1	7.4	7.6	7.8
J*V	153	290	710	1110	1520	1950
Temperature (°C)	27.8	28.5	31.0	35.4	39.3	42.5

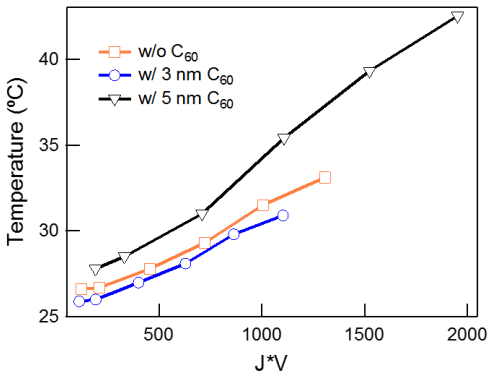

Figure 4.14 Fitting result of pixel temperature depend on the multiply of current density and applied voltage (J*V) of QD-LEDs with 0, 3, and 5 nm of C_{60} interlayer.

To verify the thermal effect on the lifetime of QD-LEDs, we measured lifetime of standard QD-LEDs (ITO//ZnO NPS//Type 1 CdSe(r = 2 nm)/$Cd_{1-X}Zn_XS$(h = 5.5 nm) QDs//CBP//MoO_x//Al) along with the additional external temperature. The applied temperature is 25, 35, and 45˚C. As depicted in Figure 4.13, the temperature on the lifetime of QD-LEDs mainly influenced on Stage II term. The result is consistent with the analysis of various operational stability resulting that the evidence of thermal energy affects rarely affect to the Stage I but mainly affect to the Stage II term.

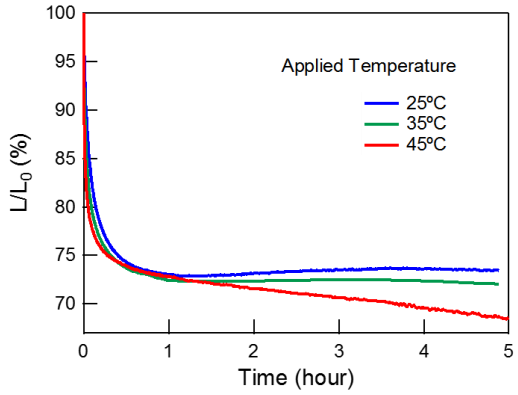

Figure 4.15 Lifetime of QD-LEDs with applied temperature form 25˚C to 45˚C.

4.7 Summary

In summary, we have assessed comprehensive study across spectroscopic analysis on the QD emissive layer and optoelectronic characterization on working devices under varying operation conditions which enabled us to understand the key factors that are responsible for the device degradation. The quantitative assessment of operational stability in QD-LEDs with all-else-being-equal conditions unveiled the effect of operational conditions (Applied current density, applied voltage, and charge imbalance factor) on the device stability. The device efficiency drop at Stage I is attributed solely to the charge injection imbalance into QDs. The device efficiency loss at Stage II is also attributed mainly to the charge injection imbalance, and further exacerbated by the increase in the operation voltage. The temperature rise during device operation was measured by IR-camera to define the temperature variation on the operation conditions. The lifetime test assessed by additional external temperature showed consistent result that Stage I disregard the effect of temperature however Stage II is influenced by additional temperature due to the HTL degradations.

Chapter 5

Conclusion

In this thesis, we devised QD-LEDs employing hybrid CTLs with enhanced charge injection balance and characterized the device performance of QD-LEDs. Insertion of a thin C_{60} interlayer at the interface between organic HTL and MoO_X//Al promotes the hole current, an inferior carrier than its counterpart, by eliminating the universal energy barrier, and lowers the operation voltage of QD-LEDs. As a consequent of enhanced charge balance in the QD emissive layer within working devices and reduced operation voltage, QD-LEDs employing C60 interlayer exhibit significantly enhanced device efficiency and operation stability.

First, we demonstrate QD-LEDs assisted by various deep HOMO hole injection interlayer to enhance to hole injection property. Thin HIIL layer eliminate the electrical dipoles between CBP and MoO_x, resulting reduced the universal ohmic contact which existed by pinning effect of metal oxide and organic materials.

Efficiency and lifetime of QD-LEDs enhanced evidently with the insertion of thin (~ 5 nm) HIIL. To define the origin of device enhancement, the electrical characteristics were analyzed by impedance spectroscopy and temperature analysis. We fabricated hole only devices without QDs to specifically observe interface component (Between CBP and MoO_x) and the cole-cole plot fitting result showed that the insertion of HIIL high reduce the interface resistance and increase interface capacitance, which defines as mobile charge carriers. Lastly the activation energy calculated by temperature experiment ensured us the abrupt decrease in HODs and QD-LEDs assisted by deep HOMO interlayer.

Comprehensive study across spectroscopic analysis on the QD emissive layer and optoelectronic characterization on working devices under varying operation conditions enable us to understand the key factors that are responsible for the device degradation. The quantitative assessment of operational stability in QD-LEDs with all-else-being-equal conditions unveiled the effect of operational conditions (Applied current density, applied voltage, and charge imbalance factor) on the device stability. The device efficiency drop at Stage I is attributed solely to the charge injection imbalance into QDs. The device efficiency loss at Stage II is also attributed mainly to the charge injection imbalance, and further exacerbated by the increase in the operation voltage. The temperature rise during device operation was measured by IR-camera to define the temperature variation on the operation conditions. The lifetime test assessed by additional external temperature showed consistent result that Stage I disregard the effect of temperature however Stage II is influenced by additional temperature due to the HTL degradations.

In conclusion, this thesis offers a strategy to enhance QD-LEDs and unveiled the relation between operational conditions and stability of devices. These results lie in a same line with previous studies that reported the impact of charge injection balance

on the device performance, and suggest that the equalized charge injection will enable complete eradication of device degradation factors and promise prolonged operation lifetime of QD-LEDs. Apparent next step to enhance device operational stability is realizing the complete balance in charge injection in QDs by reducing the energy barrier between HTL and the QD emissive layer. We believe that engineering at the interface between QDs and HTL will certainly enable the complete charge injection balance and a long-lived QD-LED.

Bibilography

[1] W. K. Bae, J. Lim, D. Lee, M. Park, H. Lee, J. Kwak, K. Char, C. Lee, and S. Lee,"R/G/B/Natural White Light Thin Colloidal Quantum Dot-Based Light-Emitting Devices" *Advanced Materials*, ***26***, 37 (2014)
[2] S. Coe, W. K. Woo, M. Bawendi, and V. Bulovic,"Electroluminescence from single monolayers of nanocrystals in molecular organic devices" *Nature*, ***420***, 6917 (2002)
[3] V. L. Colvin, M. C. Schlamp, and A. P. Alivisatos,"LIGHT-EMITTING-DIODES MADE FROM CADMIUM SELENIDE NANOCRYSTALS AND A SEMICONDUCTING POLYMER" *Nature*, ***370***, 6488 (1994)
[4] X. Dai, Z. Zhang, Y. Jin, Y. Niu, H. Cao, X. Liang, L. Chen, J. Wang, and X. Peng,"Solution-processed, high-performance light-emitting diodes based on quantum dots" *Nature*, ***515***, 7525 (2014)
[5] J. Kwak, W. K. Bae, D. Lee, I. Park, J. Lim, M. Park, H. Cho, H. Woo, D. Y. Yoon, K. Char, S. Lee, and C. Lee,"Bright and Efficient Full-Color Colloidal Quantum Dot Light-Emitting Diodes Using an Inverted Device Structure" *Nano Letters*, ***12***, 5 (2012)
[6] J. Lim, S. Jun, E. Jang, H. Baik, H. Kim, and J. Cho,"Preparation of highly luminescent nanocrystals and their application to light-emitting diodes" *Advanced Materials*, ***19***, 15 (2007)
[7] A. H. Mueller, M. A. Petruska, M. Achermann, D. J. Werder, E. A. Akhadov, D. D. Koleske, M. A. Hoffbauer, and V. I. Klimov,"Multicolor light-emitting diodes based on semiconductor nanocrystals encapsulated in GaN charge injection layers" *Nano Letters*, ***5***, 6 (2005)
[8] J. M. Pietryga, Y. S. Park, J. H. Lim, A. F. Fidler, W. K. Bae, S. Brovelli, and V. I. Klimov,"Spectroscopic and Device Aspects of Nanocrystal Quantum Dots" *Chemical Reviews*, ***116***, 18 (2016)
[9] H. B. Shen, Q. Gao, Y. B. Zhang, Y. Lin, Q. L. Lin, Z. H. Li, L. Chen, Z. P. Zeng, X. G. Li, Y. Jia, S. J. Wang, Z. L. Du, L. S. Li, and Z. Y. Zhang,"Visible

quantum dot light-emitting diodes with simultaneous high brightness and efficiency" *Nature Photonics*, ***13***, 3 (2019)
[10] L. Brus,"Electronic wave functions in semiconductor clusters: experiment and theory" *The Journal of Physical Chemistry*, ***90***, 12 (1986)
[11] V. I. Klimov, *Nanocrystal quantum dots*. CRC Press, 2010.
[12] Y. Shirasaki, G. J. Supran, M. G. Bawendi, and V. Bulović,"Emergence of colloidal quantum-dot light-emitting technologies" *Nature Photonics*, ***7***, 1 (2013)
[13] J. Lim, Y. S. Park, and V. I. Klimov,"Optical gain in colloidal quantum dots achieved with direct-current electrical pumping" *Nature Materials*, ***17***, 1 (2018)
[14] V. I. Klimov, S. A. Ivanov, J. Nanda, M. Achermann, I. Bezel, J. A. McGuire, and A. Piryatinski,"Single-exciton optical gain in semiconductor nanocrystals" *Nature*, ***447***, 7143 (2007)
[15] K. F. Wu, Y. S. Park, J. Lim, and V. I. Klimov,"Towards zero-threshold optical gain using charged semiconductor quantum dots" *Nature Nanotechnology*, ***12***, 12 (2017)
[16] O. V. Kozlov, Y. S. Park, J. Roh, I. Fedin, T. Nakotte, and V. I. Klimov,"Sub-single-exciton lasing using charged quantum dots coupled to a distributed feedback cavity" *Science*, ***365***, 6454 (2019)
[17] E. H. Sargent,"Colloidal quantum dot solar cells" *Nature Photonics*, ***6***, 3 (2012)
[18] C.-H. M. Chuang, P. R. Brown, V. Bulović, and M. G. Bawendi,"Improved performance and stability in quantum dot solar cells through band alignment engineering" *Nature Materials*, ***13***, 8 (2014)
[19] J. K. Jaiswal, E. R. Goldman, H. Mattoussi, and S. M. Simon,"Use of quantum dots for live cell imaging" *Nature methods*, ***1***, 1 (2004)
[20] E. F. Schubert, J. Cho, and J. K. Kim,"Light-emitting diodes" *Kirk-Othmer Encyclopedia of Chemical Technology*, (2000)
[21] H. Zhang, S. M. Chen, and X. W. Sun,"Efficient Red/Green/Blue Tandem Quantum-Dot Light-Emitting Diodes with External Quantum Efficiency Exceeding 21%" *Acs Nano*, ***12***, 1 (2018)
[22] B. S. Mashford, M. Stevenson, Z. Popovic, C. Hamilton, Z. Q. Zhou, C. Breen, J. Steckel, V. Bulovic, M. Bawendi, S. Coe-Sullivan, and P. T. Kazlas,"High-efficiency quantum-dot light-emitting devices with enhanced charge injection" *Nature Photonics*, ***7***, 5 (2013)
[23] J. Lim, Y. S. Park, K. F. Wu, H. J. Yun, and V. I. Klimov,"Droop-Free Colloidal Quantum Dot Light-Emitting Diodes" *Nano Letters*, ***18***, 10 (2018)
[24] P. Zrazhevskiy, M. Sena, and X. Gao,"Designing multifunctional quantum dots for bioimaging, detection, and drug delivery" *Chemical Society Reviews*, ***39***, 11 (2010)
[25] W. K. Bae, S. Brovelli, and V. I. Klimov,"Spectroscopic insights into the performance of quantum dot light-emitting diodes" *MRS bulletin*, ***38***, 9 (2013)
[26] D. J. H. A. D. S. C.-S. DR. JONATHAN S. STECKEL, QD VISION,"QDs Generate Light for Next-Generation Displays", (2014)
[27] I. Cho, H. Jung, B. G. Jeong, J. H. Chang, Y. Kim, K. Char, D. C. Lee, C. Lee, J. Cho, and W. K. Bae,"Multifunctional Dendrimer Ligands for High

Efficiency, Solution-Processed Quantum Dot Light-Emitting Diodes" *Acs Nano*, ***11***, 1 (2017)
[28] S. Cao, J. J. Zheng, J. L. Zhao, Z. B. Yang, C. M. Li, X. W. Guan, W. Y. Yang, M. H. Shang, and T. Wu,"Enhancing the Performance of Quantum Dot Light-Emitting Diodes Using Room-Temperature-Processed Ga-Doped ZnO Nanoparticles as the Electron Transport Layer" *Acs Applied Materials & Interfaces*, ***9***, 18 (2017)
[29] H. C. Wang, H. Zhang, H. Y. Chen, H. C. Yeh, M. R. Tseng, R. J. Chung, S. Chen, and R. S. Liu,"Cadmium-Free InP/ZnSeS/ZnS Heterostructure-Based Quantum Dot Light-Emitting Diodes with a ZnMgO Electron Transport Layer and a Brightness of Over 10 000 cd m− 2" *Small*, ***13***, 13 (2017)
[30] L. S. Wang, J. Lin, Y. S. Hu, X. Y. Guo, Y. Lv, Z. B. Tang, J. L. Zhao, Y. Fan, N. Zhang, Y. J. Wang, and X. Y. Liu,"Blue Quantum Dot Light-Emitting Diodes with High Electroluminescent Efficiency" *Acs Applied Materials & Interfaces*, ***9***, 44 (2017)
[31] J. J. Song, O. Wang, H. B. Shen, Q. L. Lin, Z. H. Li, L. Wang, X. T. Zhang, and L. S. Li,"Over 30% External Quantum Efficiency Light-Emitting Diodes by Engineering Quantum Dot-Assisted Energy Level Match for Hole Transport Layer" *Advanced Functional Materials*, ***29***, 33 (2019)
[32] C. Ippen, W. Z. Guo, D. Zehnder, D. Kim, J. Manders, D. Barrera, B. Newmeyer, D. Hamilton, C. M. Wang, C. Hotz, R. Q. Ma, J. K. Bin, B. Kim, K. Kim, K. Jang, J. Park, T. Lee, W. Y. Kim, and J. Lee,"High efficiency heavy metal free QD-LEDs for next generation displays" *Journal of the Society for Information Display*, ***27***, 6 (2019)
[33] C. Lee,"Samsung Changes the QLED Landscape", (2018)
[34] L. Qian, Y. Zheng, J. Xue, and P. H. Holloway,"Stable and efficient quantum-dot light-emitting diodes based on solution-processed multilayer structures" *Nature Photonics*, ***5***, 9 (2011)
[35] J. Pan, J. Chen, Q. Huang, Q. Khan, X. Liu, Z. Tao, Z. Zhang, W. Lei, and A. Nathan,"Size tunable ZnO nanoparticles to enhance electron injection in solution processed QLEDs" *ACS Photonics*, ***3***, 2 (2016)
[36] N. S. Han, H. S. Shim, J. H. Seo, S. Y. Kim, S. M. Park, and J. K. Song,"Defect states of ZnO nanoparticles: Discrimination by time-resolved photoluminescence spectroscopy" *Journal of Applied Physics*, ***107***, 8 (2010)
[37] R. M. Hewlett and M. A. McLachlan,"Surface structure modification of ZnO and the impact on electronic properties" *Advanced Materials*, ***28***, 20 (2016)
[38] W. Y. Ji, Y. Tian, Q. H. Zeng, S. N. Qu, L. G. Zhang, P. T. Jing, J. Wang, and J. L. Zhao,"Efficient Quantum Dot Light-Emitting Diodes by Controlling the Carrier Accumulation and Exciton Formation" *Acs Applied Materials & Interfaces*, ***6***, 16 (2014)
[39] M. D. Ho, D. Kim, N. Kim, S. M. Cho, and H. Chae,"Polymer and small molecule mixture for organic hole transport layers in quantum dot light-emitting diodes" *Acs Applied Materials & Interfaces*, ***5***, 23 (2013)
[40] W. Ji, Y. Lv, P. Jing, H. Zhang, J. Wang, H. Zhang, and J. Zhao,"Highly efficient and low turn-on voltage quantum dot light-emitting diodes by using a stepwise hole-transport layer" *Acs Applied Materials & Interfaces*, ***7***, 29 (2015)

[41] L. Qian, Y. Zheng, K. R. Choudhury, D. Bera, F. So, J. Xue, and P. H. Holloway,"Electroluminescence from light-emitting polymer/ZnO nanoparticle heterojunctions at sub-bandgap voltages" *Nano Today*, ***5***, 5 (2010)
[42] J. Zhao, J. A. Bardecker, A. M. Munro, M. S. Liu, Y. Niu, I.-K. Ding, J. Luo, B. Chen, A. K.-Y. Jen, and D. S. Ginger,"Efficient CdSe/CdS quantum dot light-emitting diodes using a thermally polymerized hole transport layer" *Nano Letters*, ***6***, 3 (2006)
[43] W. Ji, P. Jing, L. Zhang, D. Li, Q. Zeng, S. Qu, and J. Zhao,"The work mechanism and sub-bandgap-voltage electroluminescence in inverted quantum dot light-emitting diodes" *Scientific reports*, ***4***, (2014)
[44] H.-M. Kim, S. Cho, J. Kim, H. Shin, and J. Jang,"Li and Mg Co-Doped Zinc Oxide Electron Transporting Layer for Highly Efficient Quantum Dot Light-Emitting Diodes" *Acs Applied Materials & Interfaces*, ***10***, 28 (2018)
[45] J. H. Chang, P. Park, H. Jung, B. G. Jeong, D. Hahm, G. Nagamine, J. Ko, J. Cho, L. A. Padilha, D. C. Lee, C. Lee, K. Char, and W. K. Bae,"Unraveling the Origin of Operational Instability of Quantum Dot Based Light-Emitting Diodes" *Acs Nano*, ***12***, 10 (2018)
[46] V. I. Klimov, A. A. Mikhailovsky, S. Xu, A. Malko, J. A. Hollingsworth, C. A. Leatherdale, H. J. Eisler, and M. G. Bawendi,"Optical gain and stimulated emission in nanocrystal quantum dots" *Science*, ***290***, 5490 (2000)
[47] W. K. Bae, Y. S. Park, J. Lim, D. Lee, L. A. Padilha, H. McDaniel, I. Robel, C. Lee, J. M. Pietryga, and V. I. Klimov,"Controlling the influence of Auger recombination on the performance of quantum-dot light-emitting diodes" *Nature Communications*, ***4***, (2013)
[48] V. I. Klimov, A. A. Mikhailovsky, D. W. McBranch, C. A. Leatherdale, and M. G. Bawendi,"Quantization of multiparticle Auger rates in semiconductor quantum dots" *Science*, ***287***, 5455 (2000)
[49] S. Schmidbauer, A. Hohenleutner, and B. Konig,"Chemical Degradation in Organic Light-Emitting Devices: Mechanisms and Implications for the Design of New Materials" *Advanced Materials*, ***25***, 15 (2013)
[50] D. Y. Kondakov, W. C. Lenhart, and W. F. Nichols,"Operational degradation of organic light-emitting diodes: Mechanism and identification of chemical products" *Journal of Applied Physics*, ***101***, 2 (2007)
[51] D. Y. Kondakov,"Role of chemical reactions of arylamine hole transport materials in operational degradation of organic light-emitting diodes" *Journal of Applied Physics*, ***104***, 8 (2008)
[52] X. Jin, C. Chang, W. F. Zhao, S. J. Huang, X. B. Gu, Q. Zhang, F. Li, Y. B. Zhang, and Q. H. Li,"Balancing the Electron and Hole Transfer for Efficient Quantum Dot Light-Emitting Diodes by Employing a Versatile Organic Electron-Blocking Layer" *Acs Applied Materials & Interfaces*, ***10***, 18 (2018)
[53] S. Y. Cho, N. Oh, S. Nam, Y. Jiang, and M. Shim,"Enhanced device lifetime of double-heterojunction nanorod light-emitting diodes" *Nanoscale*, ***9***, 18 (2017)
[54] A. Castelli, F. Meinardi, M. Pasini, F. Galeotti, V. Pinchetti, M. Lorenzon, L. Manna, I. Moreels, U. Giovanella, and S. Brovelli,"High-Efficiency All-Solution-

Processed Light-Emitting Diodes Based on Anisotropic Colloidal Heterostructures with Polar Polymer Injecting Layers" *Nano Letters*, ***15***, 8 (2015)
[55] W. R. Cao, C. Y. Xiang, Y. X. Yang, Q. Chen, L. W. Chen, X. L. Yan, and L. Qian,"Highly stable QLEDs with improved hole injection via quantum dot structure tailoring" *Nature Communications*, ***9***, (2018)
[56] S. Chen, W. R. Cao, T. L. Liu, S. W. Tsang, Y. X. Yang, X. L. Yan, and L. Qian,"On the degradation mechanisms of quantum-dot light-emitting diodes" *Nature Communications*, ***10***, (2019)
[57] Z. W. Li,"Enhanced performance of quantum dots light-emitting diodes: The case of Al2O3 electron blocking layer" *Vacuum*, ***137***, (2017)
[58] Y. Fu, W. Jiang, D. Kim, W. Lee, and H. Chae,"Highly Efficient and Fully Solution-Processed Inverted Light-Emitting Diodes with Charge Control Interlayers" *Acs Applied Materials & Interfaces*, ***10***, 20 (2018)
[59] H. Zhang, N. Sui, X. C. Chi, Y. H. Wang, Q. H. Liu, H. Z. Zhang, and W. Y. Ji,"Ultrastable Quantum-Dot Light-Emitting Diodes by Suppression of Leakage Current and Exciton Quenching Processes" *Acs Applied Materials & Interfaces*, ***8***, 45 (2016)
[60] Y. Lee, B. G. Jeong, H. Roh, J. Roh, J. Han, D. C. Lee, W. K. Bae, J. Y. Kim, and C. Lee,"Enhanced Lifetime and Efficiency of Red Quantum Dot Light-Emitting Diodes with Y-Doped ZnO Sol–Gel Electron-Transport Layers by Reducing Excess Electron Injection" *Advanced Quantum Technologies*, ***1***, 1 (2018)
[61] J. H. Kim, C. Y. Han, K. H. Lee, K. S. An, W. Song, J. Kim, M. S. Oh, Y. R. Do, and H. Yang,"Performance Improvement of Quantum Dot-Light-Emitting Diodes Enabled by an Alloyed ZnMgO Nanoparticle Electron Transport Layer" *Chemistry of Materials*, ***27***, 1 (2015)
[62] C. Pacholski, A. Kornowski, and H. Weller,"Self-assembly of ZnO: From nanodots to nanorods" *Abstracts of Papers of the American Chemical Society*, ***224***, (2002)
[63] X. Y. Li, Y. B. Zhao, F. J. Fan, L. Levina, M. Liu, R. Quintero-Bermudez, X. W. Gong, L. N. Quan, J. Z. Fan, Z. Y. Yang, S. Hoogland, O. Voznyy, Z. H. Lu, and E. H. Sargent,"Bright colloidal quantum dot light-emitting diodes enabled by efficient chlorination" *Nature Photonics*, ***12***, 3 (2018)
[64] J.-H. Kim, C.-Y. Han, K.-H. Lee, K.-S. An, W. Song, J. Kim, M. S. Oh, Y. R. Do, and H. Yang,"Performance improvement of quantum dot-light-emitting diodes enabled by an alloyed ZnMgO nanoparticle electron transport layer" *Chemistry of Materials*, ***27***, 1 (2014)
[65] D. Zhang, M. Cai, Z. Bin, Y. Zhang, D. Zhang, and L. Duan,"Highly efficient blue thermally activated delayed fluorescent OLEDs with record-low driving voltages utilizing high triplet energy hosts with small singlet–triplet splittings" *Chemical science*, ***7***, 5 (2016)
[66] S. G. Ihn, N. Lee, S. O. Jeon, M. Sim, H. Kang, Y. Jung, D. H. Huh, Y. M. Son, S. Y. Lee, and M. Numata,"An Alternative Host Material for Long-Lifespan Blue Organic Light-Emitting Diodes Using Thermally Activated Delayed Fluorescence" *Advanced Science*, ***4***, 8 (2017)

[67] J. J. Lin, W. S. Liao, H. J. Huang, F. I. Wu, and C. H. Cheng,"A highly efficient host/dopant combination for blue organic electrophosphorescence devices" *Advanced Functional Materials*, ***18***, 3 (2008)
[68] M. C. Gather, A. Köhnen, and K. Meerholz,"White organic light-emitting diodes" *Advanced Materials*, ***23***, 2 (2011)
[69] H.-S. Lin, I. Jeon, R. Xiang, S. Seo, J.-W. Lee, C. Li, A. Pal, S. Manzhos, M. S. Goorsky, and Y. Yang,"Achieving high efficiency in solution-processed perovskite solar cells using C60/C70 mixed fullerenes" *Acs Applied Materials & Interfaces*, ***10***, 46 (2018)
[70] A. Suzuki, K. Nishimura, and T. Oku,"Effects of germanium tetrabromide addition to zinc tetraphenyl porphyrin/fullerene bulk heterojunction solar cells" *Electronics*, ***3***, 1 (2014)
[71] Y. P. Wang, Q. C. Liang, J. Y. Huang, D. G. Ma, and Y. R. Jiao,"Investigation of the hole transport characterization and mechanisms in co-evaporated organic semiconductor mixtures" *Rsc Advances*, ***7***, 45 (2017)
[72] L. S. Cui, Y. Liu, X. D. Yuan, Q. Li, Z. Q. Jiang, and L. S. Liao,"Bipolar host materials for high efficiency phosphorescent organic light emitting diodes: tuning the HOMO/LUMO levels without reducing the triplet energy in a linear system" *Journal of Materials Chemistry C*, ***1***, 48 (2013)
[73] D. Sun, Z. Ren, M. R. Bryce, and S. Yan,"Arylsilanes and siloxanes as optoelectronic materials for organic light-emitting diodes (OLEDs)" *Journal of Materials Chemistry C*, ***3***, 37 (2015)
[74] S. Rhee, J. H. Chang, D. Hahm, K. Kim, B. G. Jeong, H. J. Lee, J. Lim, K. Char, C. Lee, and W. K. Bae,""Positive Incentive" Approach To Enhance the Operational Stability of Quantum Dot-Based Light-Emitting Diodes" *Acs Applied Materials & Interfaces*, ***11***, 43 (2019)
[75] N. B. Kotadiya, H. Lu, A. Mondal, Y. Ie, D. Andrienko, P. W. Blom, and G.-J. A. Wetzelaer,"Universal strategy for Ohmic hole injection into organic semiconductors with high ionization energies" *Nature Materials*, ***17***, 4 (2018)
[76] J. Q. Zhong, H. Y. Mao, R. Wang, J. D. Lin, Y. B. Zhao, J. L. Zhang, D. G. Ma, and W. Chen,"Ionization potential dependent air exposure effect on the MoO3/organic interface energy level alignment" *Organic Electronics*, ***13***, 12 (2012)
[77] N. B. Kotadiya, H. Lu, A. Mondal, Y. Ie, D. Andrienko, P. W. Blom, and G. Wetzelaer,"Publisher Correction: Universal strategy for Ohmic hole injection into organic semiconductors with high ionization energies" *Nature Materials*, ***17***, 6 (2018)
[78] B. N. Pal, Y. Ghosh, S. Brovelli, R. Laocharoensuk, V. I. Klimov, J. A. Hollingsworth, and H. Htoon,"'Giant'CdSe/CdS core/shell nanocrystal quantum dots as efficient electroluminescent materials: strong influence of shell thickness on light-emitting diode performance" *Nano Letters*, ***12***, 1 (2011)
[79] H. Kurt and C. W. Ow-Yang,"Impedance spectroscopy analysis of the photophysical dynamics due to the nanostructuring of anode interlayers in organic photovoltaics" *physica status solidi (a)*, ***213***, 12 (2016)
[80] C.-C. Chen, B.-C. Huang, M.-S. Lin, Y.-J. Lu, T.-Y. Cho, C.-H. Chang, K.-C. Tien, S.-H. Liu, T.-H. Ke, and C.-C. Wu,"Impedance spectroscopy and equivalent

circuits of conductively doped organic hole-transport materials" *Organic Electronics*, ***11***, 12 (2010)
[81] S. Nowy, W. Ren, A. Elschner, W. Lövenich, and W. Brütting,"Impedance spectroscopy as a probe for the degradation of organic light-emitting diodes" *Journal of Applied Physics*, ***107***, 5 (2010)
[82] H. Wang, Y. Wang, B. He, W. Li, M. Sulaman, J. Xu, S. Yang, Y. Tang, and B. Zou,"Charge carrier conduction mechanism in PbS quantum dot solar cells: Electrochemical impedance spectroscopy study" *Acs Applied Materials & Interfaces*, ***8***, 28 (2016)
[83] H. Mu and D. Klotzkin,"Measurement of Electron Mobility in Alq 3 From Optical Modulation Measurements in Multilayer Organic Light-Emitting Diodes" *Journal of display technology*, ***2***, 4 (2006)
[84] W. Jia, Q. Chen, Y. Chen, L. Chen, and Z. Xiong,"Magneto-conductance characteristics of trapped triplet–polaron and triplet–trapped polaron interactions in anthracene-based organic light emitting diodes" *Physical Chemistry Chemical Physics*, ***18***, 44 (2016)
[85] H. Mu, D. Klotzkin, A. De Silva, H. P. Wagner, D. White, and B. Sharpton,"Temperature dependence of electron mobility, electroluminescence and photoluminescence of Alq3 in OLED" *Journal of Physics D: Applied Physics*, ***41***, 23 (2008)
[86] J. Park and Y. Kawakami,"Temperature-dependent dynamic behaviors of organic light-emitting diode" *Journal of display technology*, ***2***, 4 (2006)
[87] I. Cho, H. Jung, B. G. Jeong, D. Hahm, J. H. Chang, T. Lee, K. Char, D. C. Lee, J. Lim, and C. Lee,"Ligand-Asymmetric Janus Quantum Dots for Efficient Blue-Quantum Dot Light-Emitting Diodes" *Acs Applied Materials & Interfaces*, ***10***, 26 (2018)
[88] S. Nam, N. Oh, Y. Zhai, and M. Shim,"High efficiency and optical anisotropy in double-heterojunction nanorod light-emitting diodes" *Acs Nano*, ***9***, 1 (2015)
[89] J. Lim, B. G. Jeong, M. Park, J. K. Kim, J. M. Pietryga, Y. S. Park, V. I. Klimov, C. Lee, D. C. Lee, and W. K. Bae,"Influence of Shell Thickness on the Performance of Light-Emitting Devices Based on CdSe/Zn1-XCdXS Core/Shell Heterostructured Quantum Dots" *Advanced Materials*, ***26***, 47 (2014)

Publication

[1] International Journals

1. H Lee, P Tyagi, **S Rhee**, M Park, J Song, J Kim, C Lee, "Analysis of Photovoltaic Properties of a Perovskite Solar Cell: Impact of Recombination, Space Charge, Exciton, and Disorder", IEEE Journal of Photovoltaics 7 (6), 1681-1686 (2017).

2. P Tyagi, A Kumar, **S Rhee**, H Lee, J Song, J Kim, C Lee, "Plasmon-induced slow aging of exciton generation and dissociation for stable organic solar cells", Optica 3 (10), 1115-1121 (2017).

3. H Lee, **S Rhee**, J Kim, C Lee, H Kim, "Surface coverage enhancement of a mixed halide perovskite film by using an UV-ozone treatment", Journal of the Korean Physical Society 69 (3), 406-411 (2017)..

4. **S. Rhee**, J. H. Chang, D. Hahm, K. Kim, B. G. Jeong, H. J. Lee, J. Lim, K. Char, C. Lee,* and W. K. Bae, "A "Positive Incentive" Approach to Enhance Operational Stability of Quantum Dot based Light-Emitting Diode", 11 (43),

40252-40259 (2019).

5. K. An, J. Kim, M. A. Uddin, **S. Rhee**, H. Kim, K. Kang, H. Y. Woo, and C. Lee, "Germinant ZnO nanorods as a charge-selective layer in organic solar cells", Online published

[2] International Conferences

1. **S. Rhee**, H. Lee, K. Ahn, J. Song, J. Kim, and C. Lee, "Aluminum as an anode for heterojunction perovskite solar cells assisted by hole extraction layers", The International Meeting on Information Display, Busan, Korea (2015)

2. **S. Rhee,** H. Lee, K. An, J. Song, J. Kim, and C. Lee*, "Effect of HAT-CN as a hole extraction layer in inverted perovskite solar cells", 2015 MRS Fall Meeting, Boston, USA (2015).

3. **S. Rhee**, H. Lee, K. An, J. Song, J. Kim, and C. Lee*, "Study on low-cost perovskite solar cell assisted by hole extraction layer", Global Photovoltaic Conference 2016 (GPVC 16), Busan, Korea (2016).

4. **S. Rhee**, J. Kim, H. Lee, K. An, J. Kim, and C. Lee*, "Enhanced charge-carrier characteristic of Al doped TiO2 based Perovskite Solar Cells analyzed by impedance spectroscopy", International Conference on the Science and Technology of Synthetic Metals (ICSM 16), Guangzhou, China (2016).

5. **S. Rhee**, K. An, H. Lee, J. Kim, J. Kim, T. Lee and C. Lee*, "Mapping morphologically correlated photocurrent in perovskite solar cells using photoconductive atomic force microscopy", International Conference on Advanced Electromaterials (ICAE), Jeju, Korea (2017).

6. **S. Rhee**, R. Kusterer, P. Haida and C. Lee, “High Efficiency, Solution Processed QLED via 1,12-diaminododecane (DAD) Ligand Exchange”, The International Meeting on Information Display, Busan, Korea (2018)..

7. **S. Rhee**, J. Chang, K. Char, C. Lee and W. Ki Bae, J. Kwak, “Enhanced operation lifetime in quantum dot light-emitting diodes by controlling C60 hole injection layer”, The 14th International Meeting on Information Display (IMID), Gyeongju, Korea (2019) (oral).

8. **S. Rhee**, J. Chang, D. Hahm, K. Kim, H. J. Lee, K. Char, C. Lee, W. K. Bae, and J. Kwak, “ Enhanced Operational Stability of Quantum Dot based Light-Emitting Diodes by Improving Charge Injection Balance”, International Display Workshop (IDW), Sapporo, Japan (2019) (oral).

한글 초록

콜로이드성 양자점은 광소자에 사용하기에 적합한 광학적 전기적 특성을 가지고 있다. 특히나 높은 양자효율, 좁은 발광 파장대, 무기 재료의 내적 열안정성과 광안정성을 가지고 있기에 발광다이오드의 광물질로 사용하기에 적합하다. 다년간의 소재에 대한 개발과 소자 구조에 대한 연구를 통하여 양자점 발광다이오드는 소자 특성과 구조적으로 많은 발전이 있어 왔다. 현재까지 높은 효율과 수명에 도달한 양자점 발광소자이지만 아직까지 양자점 발광층으로의 전하 주입 불균형 문제를 완전히 해결하지 못하였으며, 구동 안정성의 감소 원인을 분석하는 연구가 부족한 상황이다. 본 연구에서는 정공 주입 버퍼층 삽입을 통한 양자점 발광다이오드 내부의 정공 특성을 향상시켜 전하 주입 불균형을 해소하고, 이 구조적 특이성을 활용하여 다양한 구동 조건들이 구동 안정성에 미치는 영향에 대한 연구를 진행하였다. 제어할 수 있는 모든 조건을 통일하고 정량적인 분석을 진행한 본 연구는 양자점 발광다이오드의 구동 안정성과 구동 조건의 연관 관계를 직관적으로 이해할 수 있게 도와준다.

먼저 효과적인 정공 주입을 위해 본 논문에서는 유기물 정공수송층 (CBP)과 정공주입층 (MoO_x) 사이 Pinning 효과에 의해 존재하는 0.3 eV 의 정공 주입 장벽을 없애고 양자점 발광다이오드의 전하 주입 균형을 향상시키는 연구가 진행되었다. 깊은 최고준위점유분자궤도 ((HOMO, Highest occupied molecular orbital) 에너지 준위를 가지는 물질들 (BST, HAT-CN, DPEPO, C_{60})이 소자 특성 분석에 활용되었으며, 그 중 가장 높은 효율 향상과 수명 향상 특성을 가지고 온

C_{60} 를 정공 버퍼층으로 활용하여 소자의 특성 향상을 전기적 그리고 광학적으로 분석하였다. 정공수송층과 정공주입층 사이의 에너지 장벽만을 확인할 수 있는 HOD (Hole only device)를 제작하여 저항 분석과 온도 실험을 진행하였다. 저항 분석의 결과 얇은 C_{60} 계면층을 삽입하였을 때 CBP 와 MoO_x 계면저항이 빠르게 감소하고 전하량을 나타나는 계면 정전 용량 (Capacitance)가 빠르게 증가하는 것을 확인할 수 있었다. 이러한 정공 주입 계면 특성 향상은 소자 전체에 영향을 미처 HOD 와 양자점 발광다이오드의 활성화 에너지 (Activation Energy, E_t) 감소에도 영향을 주어 결과적으로 발광다이오드의 효율과 수명 향상으로 이어진다는 것을 확인하였다.

한편 얇은 C_{60} 계면층 삽입으로 소자의 구동 특성 (전압, 전류, 전하 주입 균형)이 변한다는 특이성을 기반으로 양자점 발광다이오드의 구동 안정성 분석을 진행하였다. 일반적으로 진행되는 동일 휘도에서의 구동 안정성 비교는 구동 전류 및 구동 전압이 다르기에 구동 안정성에 미치는 요소들이 많아 정량적인 분석이 어렵다. 따라서 동일한 전류 조건 (30, 100, 200 mA/cm^2)하에 소자들의 분석을 진행하였으며, C_{60} 계면층 두께를 변화시켜 발광다이오드들이 서로 다른 구동 전압을 가지게 하여 구동 전압 및 전하 불균형 값이 구동 안정성에 미치는 영향을 확인할 수 있었다. 그 결과 초기 빠른 휘도 감소 구간인 Stage Ⅰ 은 구동 전류와 전하 주입 불균형 값에 크게 영향을 받지만 구동 전압에는 영향을 받지 않는다는 것을 확인하였으며, 이후 느린 휘도 감소 구간인 Stage Ⅱ 는 구동 전류와 전하 주입 불균형 값에 큰 영향을 받고, 한편 구동 전압 역시 부분적으로 영향을 미친다는 것을 확인하였다.

본 논문에서 개발된 양자점 발광 다이오드의 소자 구조와 구동 안정성 분석 결과는 고안정성 양자점 발광다이오드의 실현과 실질적인 상용화 제품 개발에 큰 도움이 될 것으로 생각된다.

주요어: 양자점, 양자점 발광다이오드, 구동 안정성, 전하 주입 균형, 정공 버퍼층, 플러랜

학번: 2014-21662